# A Republic, Not a Democracy:
## The John Birch Society and the Geography of the American Right

Hong Wang*

Boston University

August 18, 2026

Abstract

Through local chapters, the John Birch Society mobilized an anti-communist strand of the American right. Did this geography remain distinctive as the Society declined and the Cold War ended? Digitized 1987 rolls map 45,188 records, revealing suburban geography aligned with Goldwater, not Wallace. Most associations appear across rather than within states. Within states, evidence narrows to federal campaign contributions in 1980, lower voter registration, and greater selection into Republican primaries. This geography predicts neither Trump affinity, January 6 defendants per resident, certification objections, nor right-wing terrorism. The pattern indicates partisan absorption, not organizational persistence or direct lineage to contemporary populism.

*Keywords:* John Birch Society, organizational persistence, political violence, digitization, OCR

*JEL Codes:* N42, D72, D74, C81

*Hong Wang, `hongxi@bu.edu`. I thank Melissa Dell, Martin Fiszbein, and Robert Margo for their encouragement and advice. I thank Ryan (Muhammad) Adriansyah and Daniel Dugan for their excellent research assistance in digitizing historical documents. Special thanks to Jasmine Sykes and other archivists at the Brown University Library for helping me access the John Birch Society Collection, the BU Institute for Economic Development for funding part of this digitization, and the BU Shared Computing Cluster for providing the GPU resources.

Membership rolls and administrative records can reveal the local networks behind political outcomes, but many survive only as physical pages, scanned images, or archival records. For contemporary right-wing mobilization, this archival gap matters because recent economic and demographic shocks are easier to observe than the older organizations that may have connected those conditions to political action. Without direct measures of those networks, researchers cannot determine whether historical organizational geography adds information beyond population scale and observed contemporary correlates.

I introduce a geocoded dataset of John Birch Society (JBS) members in the 1980s. Founded in 1958 by a group of wealthy businessmen, the JBS grew into a nationwide network of secretive local chapters that shaped decades of conservative mobilization (Dallek 2023). JBS members and their organizational tactics helped Phyllis Schlafly defeat the Equal Rights Amendment (Dallek 2023; Spruill 2017), and the organization's ideological legacy—anti-communism, free-market fundamentalism, conspiratorial thinking, and the insistence that America is "a republic, not a democracy"—continues to reverberate through contemporary conservative politics.

This paper contributes to a literature on the long-run persistence of political behavior and the organizational channels that may carry it. Local political cultures can persist across generations (Voigtländer and Voth 2012; Acharya, Blackwell, and Sen 2016). Closest to my design, Satyanath, Voigtländer, and Voth (2017) use hand-collected rosters of interwar German civic associations to show that denser associational networks accelerated entry into the Nazi Party: organizational infrastructure, not grievance alone, converted discontent into mobilization. For the United States, Fryer and Levitt (2012) digitized 1920s Klan rosters to study membership and its consequences, McVeigh, Cunningham, and Farrell (2014) show that counties with 1960s Klan activism realigned toward the Republican Party over subsequent decades, and Madestam et al. (2013) find that even brief Tea Party mobilization left durable organizational residue. Relative to this work, the JBS rolls offer something rare: a comprehensive individual-record census of a national postwar right-wing membership organization, measured at fine geography, with which to evaluate a possible contemporary legacy. The paper brings a direct historical organizational measure to the persistence literature while treating its relationship with present-day politics as an empirical question.

The data come from the JBS's comprehensive 1987 membership rolls: 45,188 member records recovered from dot-matrix printout pages. Unlike the mailing-list data used by Kraft (1992), these alphabetical rolls preserve internal chapter markers, allowing me to distinguish local chapter members from members of the national "HOME" chapter while aggregating records to counties and congressional districts.

The rolls reveal a coherent historical and political geography. Outside the Deep South, Bircher strength is concentrated in counties that swung toward Goldwater in 1964; within the Deep South, the relationship reverses. Relative to their own electoral baselines, JBS counties also favored libertarian-right third-party candidates over segregationist candidacies. In later data, JBS-intensive places show elevated primary participation, Republican identification, conservative gun attitudes, and itemized federal-receipt activity through 1996. The finance result is sharpest in 1980: within states, JBS-intensive counties generated more receipt dollars and positive receipt records, and presidential receipts tilted toward Reagan rather than Anderson.

The contemporary within-state evidence identifies a related form of partisan sorting.

Three decades after the rolls, residents of JBS-intensive congressional districts are less likely to be registered overall but, among Democratic or Republican primary intenders, more likely to select the Republican primary. JBS geography also aligns with Republican-held congressional districts. It does not, however, distinguish Republican certification objectors from certifiers or predict Trump affinity, January 6 defendants per resident, or right-wing terrorism. Together, the results locate an organized base of movement conservatism within later Republican politics without making the Society a catch-all ancestor of contemporary populism or violence.

The research bottleneck for projects like this one is the cost and difficulty of converting unstructured page images into structured, analyzable data. Fryer and Levitt (2012) digitized Ku Klux Klan membership rolls from multiple archives to study who joined the 1920s Klan and its social and political impact.[1] Dell et al. (2023) demonstrate the potential of custom deep learning at massive scale, digitizing over 430 million historical newspaper articles with a modular pipeline. Dell (2025) makes a comprehensive case that custom pipelines consistently outperform both traditional methods and off-the-shelf commercial tools for extracting structured data from unstructured text and images, especially when historical sources differ sharply from modern web text.

General-purpose LLM APIs offer an appealing shortcut: send page images to a hosted model, receive fluent transcriptions, and report a character error rate estimated on a random validation sample. For research data, that error model is too thin in three ways. First, an aggregate character error rate treats errors as exchangeable, but a one-character error in a ZIP code relocates a member to a different county, while the same error in a surname is harmless for spatial analysis. Second, LLM transcription errors tend to be confabulations—well-formed records with plausible but wrong fields—so they pass both casual inspection and validity screens; a fabricated ZIP code can still be a valid ZIP code. Third, a sampled error rate cannot reveal whether mistakes are systematic—concentrated on faint pages, particular record formats, or particular regions—which is precisely the structure that converts transcription noise into spatially correlated measurement error in downstream regressions (Dell 2025). The pipeline below instead makes errors flaggable and traceable to source images, allowing verification to detect systematic patterns and bound their consequences rather than merely estimate an aggregate rate.

Recovering the JBS rolls required a custom OCR digitization and verification pipeline. I use a modular deep learning pipeline for layout detection, line segmentation, optical character recognition, parsing, and geocoding. The OCR model achieves a validation character error rate of 0.32% before final human review. More importantly, its error structure is auditable: research assistants verified lines against source images, and validation scripts screened geographic fields using ZIP-code, state, city, and alphabetical-order constraints.

The paper makes three contributions. First, I digitize and geocode the comprehensive JBS membership rolls at the individual-record level, making it possible to measure conservative organizational infrastructure directly. Second, I identify a specific route from movement conservatism into Republican politics: an organized, anti-communist, free-market, and often suburban geography associated with primary sorting and campaign finance, but not with a

[1] More recent work has compiled larger collections of KKK rosters to examine the relationship between military service and Klan participation.

general Trump-era or violent-extremist legacy. Third, I provide a practical guide to digitizing and validating structured archival membership records, while showing how an estimated population elasticity and an exposure offset can distinguish county volume from per-resident incidence in downstream count applications.

The paper proceeds as follows. Section 1 provides historical background on the John Birch Society and its connection to the anti-ERA movement. Section 2 describes the archival membership rolls. Section 3 presents the digitization and verification pipeline. Section 4 describes the geography of JBS membership. Section 6 uses the dataset to revisit existing studies of contemporary right-wing politics. Section 7 concludes by discussing interpretation, limitations, and future applications of the data.

# 1 The Birchers as Organizational Infrastructure

The John Birch Society built a national infrastructure of local chapters, recurring meetings, internal directives, front groups, newsletters, and overlapping conservative social networks. Its membership rolls offer a county-level map of conservative organizational infrastructure: the places where a secretive but nationally coordinated right-wing organization had members, routines, and potential mobilizing capacity.

Robert Welch Jr., a retired candy manufacturer from a family of Baptist preachers, founded the JBS in 1958 with several wealthy businessmen, including Fred Koch of Koch Industries, Robert Waring Stoddard of Wyman-Gordon, and Harry Lynde Bradley of the Allen-Bradley Company. The organization took its name from John Birch, a Baptist missionary and U.S. military intelligence officer killed by Chinese Communist forces in 1945, whom Welch regarded as the first American casualty of the Cold War. Welch envisioned the JBS as "humanity's last hope" against what he believed was an imminent Communist takeover of the United States, orchestrated by a shadowy cabal of elites pursuing a New World Order.

The JBS combined free-market ideology with conspiratorial anti-communism in ways that distinguished it from mainstream conservatism. The JBS promoted the view that Republican President Dwight Eisenhower was part of the Communist conspiracy, that fluoridation of public water was a Communist plot to control Americans, and that the Civil Rights Movement and Martin Luther King Jr. were instruments of Soviet subversion.[2] In the 1970s, the Society also supported laetrile as a cancer treatment: JBS bookstores sold pro-laetrile materials, and Birchers held leading roles in its advocacy network (Markle, Petersen, and Wagenfeld 1978). The JBS also popularized the claim that America is "a republic, not a democracy," an idea that continues to appear in contemporary conservative discourse.

The organization's tactics were as important as its ideology. Welch, drawing on his background in marketing, understood the importance of packaging political ideas for mass consumption. The JBS maintained a prescriptive monthly bulletin and published *American Opinion*, through which national leadership directed the activities of local chapters. The organization expected members to attend monthly meetings, though enforcement varied. The JBS capped local chapters at twenty members to preserve secrecy, a structure explicitly modeled on small Communist cells. The JBS also created front organizations with innocuous

[2]The fluoridation conspiracy was satirized in Stanley Kubrick's 1964 black comedy *Dr. Strangelove*, where General Jack D. Ripper warns that fluoridation threatens Americans' "precious bodily fluids."

names, allowing members to pursue organizational goals without the stigma of direct association (Dallek 2023; Spruill 2017). Chapter routines, front groups, and national directives make JBS membership a plausible measure of local organizational capacity.

The JBS initially drew members from the upper echelons of American society, including wealthy businessmen and their social circles, before expanding to white upper-middle-class professionals such as doctors and dentists.[3] Members paid dues that varied by gender: the JBS charged men $24 per year, approximately $260 in 2024 dollars, while women paid half that amount. Mainstream conservative figures attempted to distance the movement from the JBS—William F. Buckley Jr.'s *National Review* publicly denounced its more extreme claims—yet these denunciations appear to have deepened the commitment of existing members (Dallek 2023).[4]

The JBS was especially active in suburban conservative mobilization. In Pasadena and Orange County, the organization opposed school integration while also rallying economic elites against labor unions and the welfare state (McGirr 2001). Together, cultural conservatism, economic libertarianism, and grassroots suburban organizing anticipated strategies that would later become central to the modern Republican coalition. The key implication for this paper is that JBS membership reflected local social and political networks as well as national ideological discourse.

Phyllis Schlafly's campaign against the Equal Rights Amendment illustrates the connection between JBS networks and broader conservative mobilization. Archival correspondence and JBS internal records indicate that Schlafly belonged to the John Birch Society, though she later denied it, and that she resigned strategically in 1964 to prevent *A Choice Not an Echo* from being associated with the organization during the Goldwater campaign.[5] Dallek (2023) documents JBS members leaving the official rosters while maintaining close informal ties to the organization.

Through STOP ERA, Eagle Forum, and *The Phyllis Schlafly Report*, Schlafly united evangelical Protestant and Catholic women against ERA ratification. She personally selected state chairwomen for STOP ERA, drawing on overlapping contacts from the National Federation of Republican Women, the National Council of Catholic Women, the Daughters of the American Revolution, the Goldwater campaign, and other conservative organizations (Spruill 2017) .

Several state chairs drew on JBS networks to build their operations, although the extent to which Schlafly herself directed this is not documented. Dorothy (Dot) Malone Slade, a JBS member who knew Schlafly through the NFRW, led North Carolina and invited fellow JBS members to help. Beverly Findley, a former JBS member, led Oklahoma with Ann Patterson

[3]Kraft (1992) found that physicians and dentists were disproportionately represented in the JBS mailing list: 3.54% of his sample held the title "Dr" or "MD," compared to approximately 0.25% of the general population who were physicians.

[4]Archival documents show that the JBS revoked the membership of individuals it found to be associated with the KKK.

[5]In a December 5, 1959 letter to Verne Kaub of the American Council of Christian Laymen, Schlafly wrote that she and her husband "both joined promptly after the Chicago meeting." The February 1960 *JBS Bulletin* described her as "a very loyal member." In her oral history, however, Schlafly said only that she had attended "a seminar that Robert Welch spoke at in Chicago" (DePue 2011). In an August 19, 1964 letter to Mrs. Tom Anderson, a JBS National Council member's wife, Welch confirmed that the decision not to promote the book through JBS bookstores was at Schlafly's request (Lazar 2020).

and worked with JBS members in planning anti-ERA hearings. In Mississippi and Oklahoma, anti-ERA organizing drew on the State Farm Bureau, which had close institutional ties to the JBS. In Utah, JBS women organized against the ERA through a front group called HOTDOG—Humanitarians Opposed to Degrading Our Girls (Spruill 2017).[6]

# 2 The 1987 Membership Rolls

The data for this project come from the John Birch Society records held at the John Hay Library at Brown University. When the JBS relocated its headquarters from Belmont, Massachusetts, to Appleton, Wisconsin, in 1989, Chip Berlet of Political Research Associates (PRA) recovered discarded headquarters materials from a dumpster outside the Belmont office; PRA later donated those materials to Brown (Kraft 1992). The Brown materials include several membership-related sources. Kraft (1992) analyzed a JBS mailing list, then held at PRA and labeled JMS 344, which included first-class postage, second-class postage, and complimentary-list sections.[7]

The source digitized here is distinct from the mailing list analyzed by Kraft (1992).[8] I digitize the JBS's alphabetical membership rolls, which organize members by surname, not postal class. The rolls appear to be a comprehensive internal membership record as of 1987 and contain 45,188 records across 1,870 scanned page images of continuous-feed dot-matrix printout.[9] In total, the rolls contain 99,183 text lines. Appendix Table 6 reports 638 joint spousal records, usually entries beginning with "Mr & Mrs." The dataset therefore counts membership records, not unique individuals. Unlike state totals or sampled ZIP-code data, the rolls preserve individual records and internal chapter markers while supporting county- and district-level aggregation. In Section 4, I use that structure to measure conservative organizational presence before the contemporary populist period.

# 3 Digitization and Verification

The central digitization challenge was spatial accuracy. The empirical analyses depend on county and district assignment, so an OCR error in a ZIP code, city, or state can move a member to the wrong place. I therefore designed the pipeline around auditable accuracy: each stage produces intermediate outputs that reviewers can inspect, correct, and link back to the source image.

The pipeline has four stages. First, layout detection identifies the region of each page that contains membership records. Second, line detection segments that region into individual text-line images. Third, OCR reads the content of each line. Fourth, post-processing parses

[6]In 1977, JBS leader John F. McManus claimed the JBS had members "in leadership positions in every state where the ERA was scotched" (Spruill 2017).

[7]The second-class postage entries begin with foreign addresses before proceeding to domestic members, corresponding to the categories described in his study. Excluding the complimentary list, Kraft counted 21,305 individual and joint spousal memberships and 58 foreign members.

[8]I did not digitize the mailing-list sections used in that study.

[9]The page count refers to scanned PDF page images, not to the printout's internal page numbers, which do not correspond consistently to the alphabetical sequence of entries.

the OCR output into structured member records and assigns geographic units. Figure 1 summarizes the workflow.

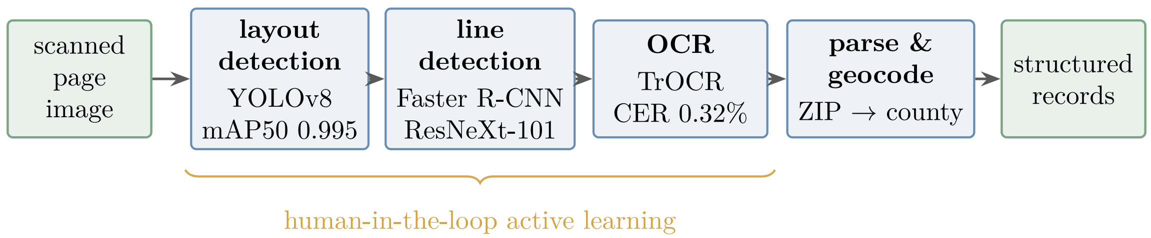


Figure 1: Pipeline architecture and division of labor. The brace marks the stages where active learning lowers marginal labeling costs; parsing and geocoding are deterministic post-processing steps, not learned predictions.

## 3.1 Layout Detection

Layout detection separates the membership-record area from headers, page numbers, margins, and other non-data material. Although the relevant region is visually obvious to a human, isolating it prevents later stages from treating page artifacts as member records. I treated layout detection as a human-in-the-loop task, using Label Studio (Tkachenko et al. 2020) with a fine-tuned small YOLOv8 model (Jocher, Chaurasia, and Qiu 2023). Initial hand labels generated model predictions; I folded corrected predictions back into training.

The layout stage required labeling 1,460 of 1,870 page images. The final model achieved mAP50 of 0.995 and mAP50–95 of 0.962, indicating near-perfect recovery of the data region. Because the target region is large and visually regular, a small YOLOv8 model trained with default hyperparameters was sufficient.

## 3.2 Line Detection

Line detection was the most technically demanding stage. Each page contains roughly 53 text lines, and each line is long and narrow, approximately $16 \times 659$ pixels. The line geometry is poorly suited to object detectors optimized for compact natural-image objects. A YOLOv8 model, successful in the layout stage, performed poorly for line detection, reaching only 47% mean average precision.

The failure reflected box geometry, not computation alone. Text lines require proposal boxes that are many times wider than they are tall. I therefore switched to Detectron2 (Wu et al. 2019) with a Faster R-CNN architecture and a ResNeXt-101 backbone pretrained on COCO (Lin et al. 2014). I customized the anchor ratios to 0.02–0.04, corresponding to boxes 25 to 50 times wider than tall. Figure 2 illustrates why this change was necessary.

I trained the line-detection model on 7,732 page crops derived from the layout labels. Over training, total loss fell from 2.18 to 0.17, RPN classification loss fell from 0.686 to below 0.001, and foreground classification accuracy rose from 14.3% to 96.7%. I exported model predictions directly into the same Label Studio project where reviewers labeled and corrected line boxes.

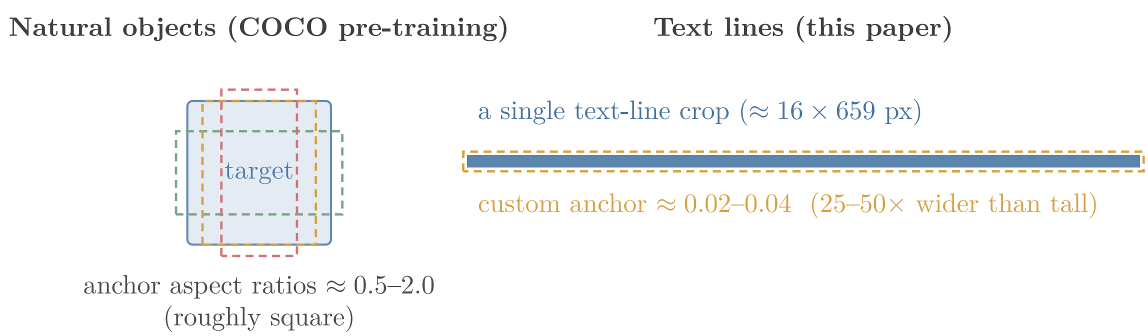


Figure 2: Anchor geometry, not model size, is the binding design choice for line detection. Natural-image pretraining supplies useful visual features, but the proposal network must be re-tuned to the long, thin boxes that membership-roll text lines occupy.

## 3.3 Optical Character Recognition

After line segmentation, OCR reads the text from each line image. I fine-tuned the TrOCR model (Li et al. 2023), a transformer-based OCR architecture, on the visual characteristics of the JBS dot-matrix printout. Early tests with generic OCR systems, including Apple OCR, helped bootstrap initial labels but produced too many errors for final data construction. Those predictions also revealed the source's characteristic error structure: visually similar dot-matrix characters, dropped punctuation, and inconsistent spacing.

At all stages, I used an active-learning workflow. Research assistants corrected batches of line images; I added the corrected lines to the training set; the updated model generated predictions for the next batch. As accuracy improved, each batch required fewer corrections. Human review remained constant, but the nature of the task shifted as the amount of human typing declined sharply over time.

The OCR training set advanced sequentially through the alphabet. Random sampling would better estimate population-level error, but the goal was full-corpus digitization; the fixed record format and visual features do not vary systematically by surname.

The final OCR training and validation set contains 82,797 corrected text lines, with 74,517 used for training and 8,280 for validation. After 58 passes over the training data, the model achieved a validation character error rate of 0.32%, or fewer than one incorrect character per 300 characters on average. The final model processed the remaining 16,386 line crops, and research assistants verified those lines against the source images.[10] Table 1 reports the decline in character error as the training set expanded.

## 3.4 Post-Processing and Geocoding

The raw OCR output is a sequence of text lines. I link those lines into member records and parse them into fields. Each JBS record generally spans two lines: the first contains the surname, given name, household code, salutation, and street address; the second contains the city, state, ZIP code, chapter marker, and administrative codes. I infer gender from

[10] Additional training details for all pipeline stages, including learning rate, batch size, anchor sizes, and evaluation schedule, appear in Appendix Table 5.

Table 1: OCR active-learning returns as labeled lines increase

| Labeled lines | Corpus % | Validation CER % |
|---|---|---|
| 2,415 | 2.4% | 2.95 |
| 5,889 | 5.9% | 1.85 |
| 9,600 | 9.7% | 1.19 |
| 82,797 | 83.5% | 0.32 |

*Notes:* CER is measured on a 20% held-out validation set. The total corpus contains 99,183 lines.

salutations such as Mr., Mrs., Ms., and Miss. Because the rolls use a regular fixed-position format, parsing depends on reproducibility and field preservation. The parser preserves tokens in a structured schema, retains administrative codes, and assigns counties using ZIP Code Tabulation Area (ZCTA) crosswalks. Figure 3 shows a representative record parse.

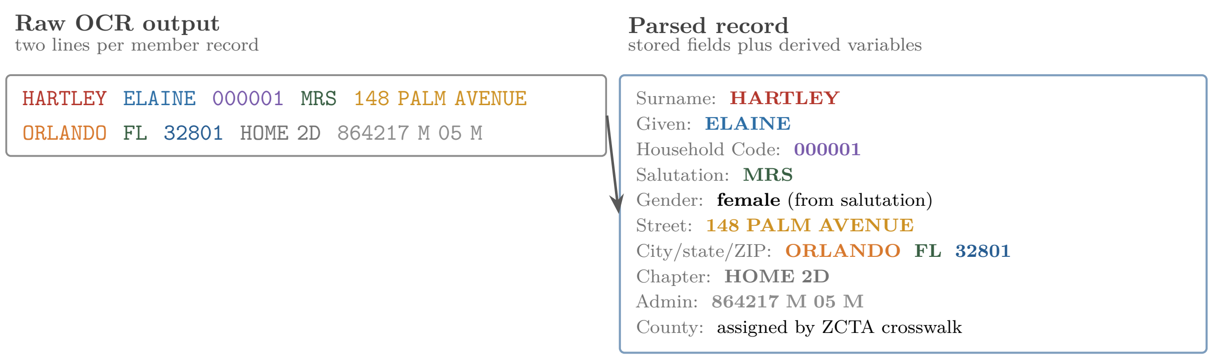


Figure 3: Fixed-position parsing converts two OCR lines into analyzable fields. The fictitious example preserves the record structure while replacing personal identifiers. The parser derives gender from salutations, retains the household code field, keeps chapter markers distinct from administrative codes, and assigns county after ZIP parsing through a ZCTA crosswalk.

## 3.5 Verification and Error Auditing

The verification design has two layers. First, research assistants checked every text line against the source image. Hence, no line entered the final dataset without human review; each parsed field therefore traces back to a line that a research assistant typed or checked against the original image.

Second, the pipeline exploits the structure of the records to catch residual errors. The most common OCR confusions involve visually similar characters in dot-matrix print, especially 0/O, 1/I, and 5/S. Dot-matrix confusions can corrupt names and administrative fields, but geographic errors are most consequential for this paper. Validation scripts checked ZIP codes against valid entries, state abbreviations against a fixed list, and city–ZIP combinations against known geographic matches, then flagged failed records for manual review. The alphabetical ordering of the rolls provides a final structural check. Because pages proceed by surname, any record outside the expected alphabetical range of its page indicates a linking, parsing, or OCR problem.

The final dataset passes this check with no breaks across all 1,870 pages. The verification strategy makes county- and district-level analysis possible. The relevant claim is that the pipeline made errors visible, bounded, and correctable, producing a set of geocoded membership records with spatial assignments traceable to verified source lines.

# 4 The Geography of JBS Membership

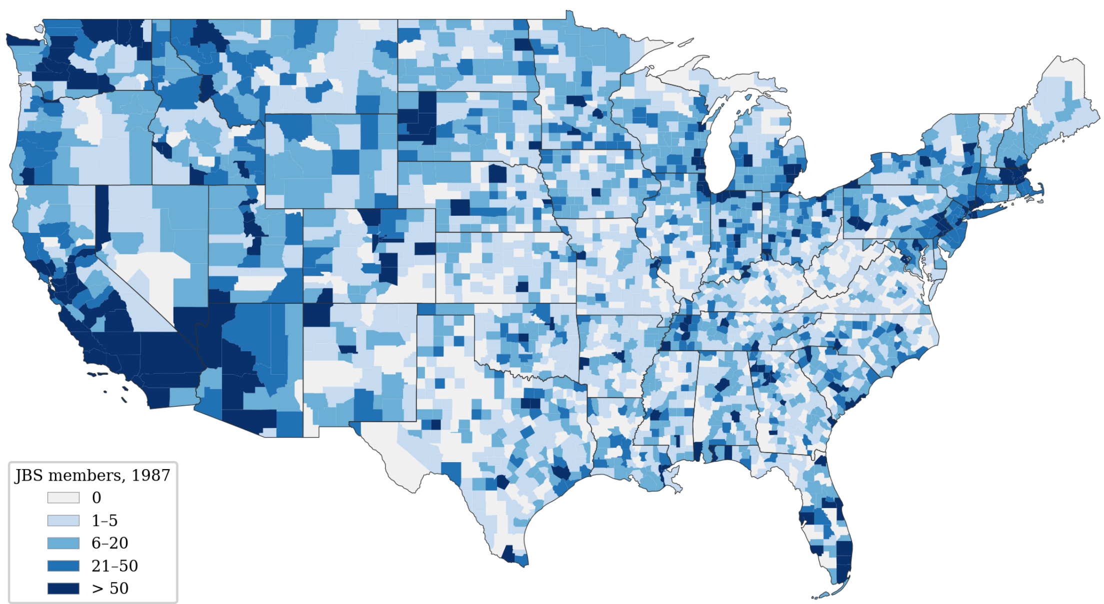


Figure 4: County-level geography of JBS membership in the 1987 rolls. The map displays the historical organizational stock used in the empirical applications below.

The verified rolls contain 45,188 member records, of which 45,137 (99.9%) crosswalk to a county. The outcome-analysis universe contains 45,091 records across 2,456 U.S. counties in all 50 states.[11] Because some records list married couples jointly, the number of individuals represented is somewhat higher than the number of records. The county distribution is highly skewed: among counties with at least one member, the median had seven, while Los Angeles County alone had 1,582. Overall, the JBS had at least one recorded member in 78% of U.S. counties.

[11]Fifty-one records do not match the ZCTA–county crosswalk. Another 46 geocode to areas outside the county analysis universe: San Juan, Puerto Rico; St. Croix, U.S. Virgin Islands; and the Chugach and Copper River census areas created by the 2019 split of Alaska's Valdez–Cordova area.

## 4.1 Geographic Distribution

The absolute geography of membership reflects the organization's known strongholds. California had the largest number of records (5,726), consistent with historical accounts of JBS organizing in Orange County and the Los Angeles suburbs (Dallek 2023; McGirr 2001). Texas ranked second (2,446), followed by Georgia (1,822), Indiana (1,715), and Florida (1,649).

The rolls map organizational presence, not conservative population alone. JBS members received communications, could attend local meetings, and could connect through chapters, front groups, and overlapping conservative networks. The measure therefore captures a historical stock of organizational infrastructure, not a contemporaneous vote outcome.

Appendix Table 6 summarizes membership by gender. Men outnumbered women roughly 3:2, consistent with the JBS's origins in male business networks. The substantial female membership also fits historical accounts of women sustaining local JBS organizing even as men dominated much of the national leadership (Dallek 2023).

## 4.2 Validation Against Prior Work

The geography of the digitized rolls is qualitatively consistent with the leading states reported by Kraft (1992), even though the underlying source differs. Kraft's smaller active mailing list placed California, Texas, and Florida first, second, and third, with 2,648, 1,232, and 1,154 members, respectively. Those states are also among the five largest in the alphabetical rolls digitized here: California has 5,726 records, Texas 2,446, and Florida 1,649. Because the two sources cover different internal lists and membership universes, this agreement is a face-validity check on the broad geography, not a claim that their state totals are directly comparable.

## 4.3 Distinguishing the 1987 JBS from 1964 Goldwater Geography

A natural concern is that JBS membership may reproduce the geography of Goldwater-era conservative mobilization, especially in Southern California (Dallek 2023; McGirr 2001). County-level presidential returns suggest otherwise. I measure Goldwater-era mobilization as the swing in the Republican two-party share from Nixon in 1960 to Goldwater in 1964. Nationally, the relationship between the Goldwater swing and 1987 JBS membership is weak ($r = -0.07$) because two much stronger regional patterns pull in opposite directions. Outside the South, the swing is positively correlated with later JBS membership ($r = 0.14$, $p < 10^{-9}$), consistent with a free-market, anti-communist conservative tradition. In the Deep South, the relationship is negative ($r = -0.26$, $p < 10^{-7}$),[12] reflecting a different regional coalition organized around civil-rights backlash and rural Black Belt politics.

Read alongside the JBS's historically documented suburban organizing in places such as Pasadena and Orange County (McGirr 2001), the regional decomposition supports interpreting the rolls as a measure of one strand of conservative organizational infrastructure rather than generic conservative partisanship. The JBS measure captures organized, anti-communist,

[12]The Deep South pattern is not driven by Alabama's unusual 1964 ballot context: excluding Alabama yields a similar negative correlation between the Goldwater swing and later JBS membership.

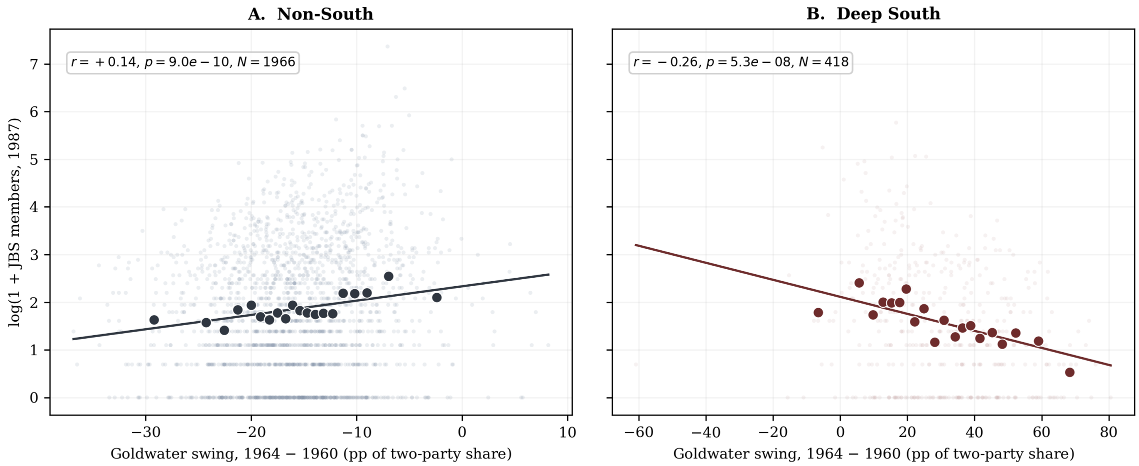


Figure 5: Regional decomposition of the county-level relationship between the Goldwater swing (Republican two-party share in 1964 minus 1960) and 1987 JBS membership. Binned means (20 quantile bins) overlay the county scatter. Outside the South the swing is positively associated with later JBS membership ($r = 0.14$, $p < 10^{-9}$); in the Deep South the relationship is negative ($r = -0.26$, $p < 10^{-7}$).

free-market, and often suburban conservatism; it does not simply reproduce the rural Black Belt geography of the Deep South's Goldwater swing. Figure 5 summarizes this distinction.

## 4.4 Denominational Geography

A second source locates the same distinction without using electoral returns at all. Table 2 correlates county JBS intensity with county adherence rates by religious body, taken from the 1990 wave of the Religious Congregations and Membership Study (Grammich et al. 2018). All 3,093 county units enter; counties absent from the rolls are treated as zeros rather than as missing.

Unconditionally and net of county population, the rolls are strongly *anti*-evangelical (−0.191) and *anti*–Southern Baptist (−0.210), and positively associated with the Lutheran Church–Missouri Synod (0.125) and the Latter-day Saints (0.189). That is the denominational counterpart of the regional pattern above: the geography of the rolls is not the geography of Southern evangelical Protestantism.

The third column is the one to be careful about. Adding a South indicator collapses the Missouri Synod, Southern Baptist, evangelical, mainline, and historically Black Protestant coefficients to something close to zero. These bodies are regionally sorted, so "not Southern Baptist" and "not Southern" are largely the same fact rather than two independent pieces of evidence. The denominational data locate the regional pattern in an independent source; they do not confirm it independently, and the text should not claim that they do.

Two associations survive the regional control and are therefore genuinely denominational. Latter-day Saints adherence remains the strongest coefficient in the table (0.156), and the Churches of Christ and Assemblies of God coefficients flip from negative to positive once region is netted out (−0.053 → 0.048 and 0.053 → 0.049). Outside the South, these bodies sit with the rolls rather than against them.[13]

Table 2: The denominational geography of the 1987 membership rolls

| | Unconditional correlation | Net of log population | Net of log pop. and South |
|---|---|---|---|
| Lutheran Church–Missouri Synod | 0.005 | 0.125*** | 0.035~ |
| Wisconsin Evangelical Lutheran Synod | 0.042* | 0.077*** | 0.034~ |
| Latter-day Saints | 0.101*** | 0.189*** | 0.156*** |
| Presbyterian Church in America | 0.031~ | −0.008 | 0.030~ |
| Mainline Protestant | −0.106*** | 0.080*** | −0.005 |
| Catholic | 0.168*** | 0.107*** | 0.008 |
| Jewish | 0.284*** | 0.021 | −0.004 |
| Churches of Christ | −0.123*** | −0.053** | 0.048** |
| Assemblies of God | −0.009 | 0.053** | 0.049** |
| Evangelical Protestant | −0.266*** | −0.191*** | −0.027 |
| Southern Baptist Convention | −0.237*** | −0.210*** | −0.029 |
| Historically Black Protestant | −0.069*** | −0.131*** | −0.014 |

*Notes.* Correlations between log(1 + JBS members, 1987) and county adherence rates by religious body, from the ARDA Religious Congregations and Membership Study, 1990 wave. 3,093 county units; counties absent from the membership rolls enter at zero rather than as missing. Partial correlations are computed by residualising both variables on the stated controls. $^{\sim}p < 0.10$; $^{*}p < 0.05$; $^{**}p < 0.01$; $^{***}p < 0.001$.

# 5 From Movement Conservatism to Republican Politics, 1948–2021

The Society was organized against communism, and its 1987 rolls locate members just before the Soviet collapse removed that common enemy. The historical question is what political form, if any, this geography assumed afterward. Across election returns, campaign-finance records, and surveys, the recurring association is with Republican partisan and primary politics rather than generalized participation or Trump-era populism.

I distinguish national from within-state geography. The national specification describes how respondents, counties, and districts in more JBS-intensive places differ across the country; the state-fixed-effects specification compares places governed by the same state institutions. Both are descriptive: their divergence locates the scale of an association rather than establishing organizational transmission. The evidence comes from county presidential returns, FEC-classified itemized receipts, the Cumulative Cooperative Election Study (CES), Nationscape, and the ANES (Algara and Amlani 2021; Federal Election Commission 2026; Kuriwaki 2026; Ansolabehere, Schaffner, and Luks 2021; Tausanovitch and Vavreck 2021;

[13]The Missouri Synod coefficient is sample-sensitive: it is 0.23 in the 216 metropolitan-skewed ANES counties, but 0.125 nationally net of population and 0.035 net of region. I therefore do not treat it as an independent confessional-Lutheran association.

American National Election Studies 2022). The exposure is standardized $\log(1 + \text{JBS records})$ at the relevant geographic level. Models retain the source-specific weights, controls, time effects, and geographic clustering described in Appendix Section 8.6.

Multiplicity adjustments cover the complete outcome families rather than only the estimates discussed below. Romano–Wolf step-down values use 4,999 shared cluster-influence draws within the 48-outcome CES, 21-outcome Nationscape, and eight-outcome FEC families (Romano and Wolf 2005). Most of the national CES profile and post-1980 FEC pattern does not survive comparisons within states; the narrower within-state results concern 1980 receipt activity and later registration and Republican-primary sorting. Appendix Tables A1–A4 report all outcomes, nulls, and candidate-level tests.

## 5.1 Participation and Itemized Federal Receipts

The clearest national behavioral alignment is selective participation in primaries. A one-standard-deviation increase in JBS intensity is associated with 2.52 percentage points more validated primary turnout, compared with 0.79 points for general-election turnout; the respondent-level difference is 1.73 points. These associations disappear with state fixed effects: the matched primary-turnout estimate is $-0.09$ points. The national pattern therefore reflects cross-state sorting rather than a detectable within-state county gradient in primary participation.

The FEC archive supplies the historically bounded result in Table 3. Receipt dollars survive familywise correction nationally in 1980, 1992, and 1996, and positive receipt records do so in 1980 and 1996. Within states, only the 1980 dollar and record associations remain; both 2012 outcomes are null. County income and education reduce the mean national dollar coefficient by 59%, so measured affluence accounts for a substantial part of the receipt geography. The records count positive transactions rather than unique donors.

Candidate allocation is narrower still. Across a joint family of nineteen candidate-level and candidate-share tests, the only surviving insurgent-share estimate is a lower Anderson share relative to Reagan in 1980. No Perot, Buchanan, Ron Paul, or Libertarian level or share survives. The finance evidence therefore identifies an older Reagan–Anderson divide, not a general or durable pattern of insurgent fundraising. Appendix Table A4 and the supplementary figures report the complete candidate, control, and annual-turnout results.

Table 3: JBS membership, FEC receipts, and primary participation: national specifications

*Panel A. FEC itemized individual receipts*

| | Receipt dollars per capita | | Positive receipt records per capita | | |
|---|---|---|---|---|---|
| Cycle | $\beta$ | RW $p$ | $\beta$ | RW $p$ | Counties |
| 1980 | 0.112*** | <0.001 | 0.091*** | 0.001 | 3,084 |
| | (0.023) | | (0.027) | | |
| 1992 | 0.063** | 0.007 | 0.034 | 0.379 | 3,088 |
| | (0.021) | | (0.027) | | |
| 1996 | 0.096*** | <0.001 | 0.087*** | 0.001 | 3,088 |
| | (0.022) | | (0.026) | | |
| 2012 | 0.025 | 0.379 | −0.008 | 0.749 | 3,088 |
| | (0.018) | | (0.023) | | |

*Panel B. Weighted CES 2006–2020*

| Outcome | $\beta$ | RW $p$ | Respondents |
|---|---|---|---|
| Validated primary turnout | 2.523*** | <0.001 | 341,618 |
| | (0.391) | | |
| Validated general-election turnout | 0.793* | 0.450 | 341,607 |
| | (0.348) | | |
| Primary minus general-election turnout | 1.728*** | <0.001 | 341,606 |
| | (0.352) | | |
| Registered Republican × primary turnout | 0.818* | 0.352 | 263,705 |
| | (0.338) | | |
| Republican share among D/R primary voters | 4.090*** | <0.001 | 35,002 |
| | (0.880) | | |
| Interest in politics† | −0.003 | 1.000 | 429,919 |
| | (0.005) | | |

*Notes.* Standard errors clustered by county are in parentheses beneath estimates; JBS intensity is standardised over unique counties. Panel A uses FEC-classified itemized-individual receipts. Dollar outcomes are $\log(1 + \max\{x, 0\})$, standardised within cycle after signed records are aggregated to county net amounts. "Records" means positive itemized receipt records, not unique donors. Panel B uses the CES cumulative survey weight. Binary outcomes are in pp; †marks the standardised interest scale. Voter-file party registration is unavailable in 2008 and 2010, so the joint registered-Republican/validated-primary-turnout outcome excludes those years. All models include county religious composition, log contemporaneous population, South, annual log per-capita income and bachelor's share; CES models add individual age, education, income, race, gender and religion plus year fixed effects. RW $p$ is the Romano–Wolf step-down value from 4,999 shared cluster influence-score multiplier draws within the fixed eight-outcome FEC or 48-outcome CES family. Appendix Table A1 reports the matched state-fixed-effects estimates. Stars use the conventional cluster-robust test: $^{\sim}p < 0.10$; $^{*}p < 0.05$; $^{**}p < 0.01$; $^{***}p < 0.001$.

## 5.2 Third-Party Voting, 1948–2020

Third-party presidential voting distinguishes among varieties of conservatism without relying on survey responses. Figure 6 reports a county and election-year fixed-effects event study covering 58,875 county-elections. Relative to each county's own third-party baseline, JBS-intensive counties voted less for George Wallace in 1968 ($\beta = -0.239$) and more for Anderson and Clark in 1980 (0.127), Perot in 1992 (0.067), and Johnson and other minor candidates in 2016 (0.075). The 1996 Perot coefficient is negative, so this is not a durable Perot constituency.

The more important bound predates the organization: the 1948 Thurmond coefficient is also negative ($-0.080$), a decade before the Society's founding. The rolls thus locate a libertarian-right rather than Wallace-style geography, but they also mark a political culture into which the Society recruited rather than one it necessarily produced. That pre-founding result is the strongest reason to interpret the later associations descriptively. Appendix Table A2 reports the numerical series.

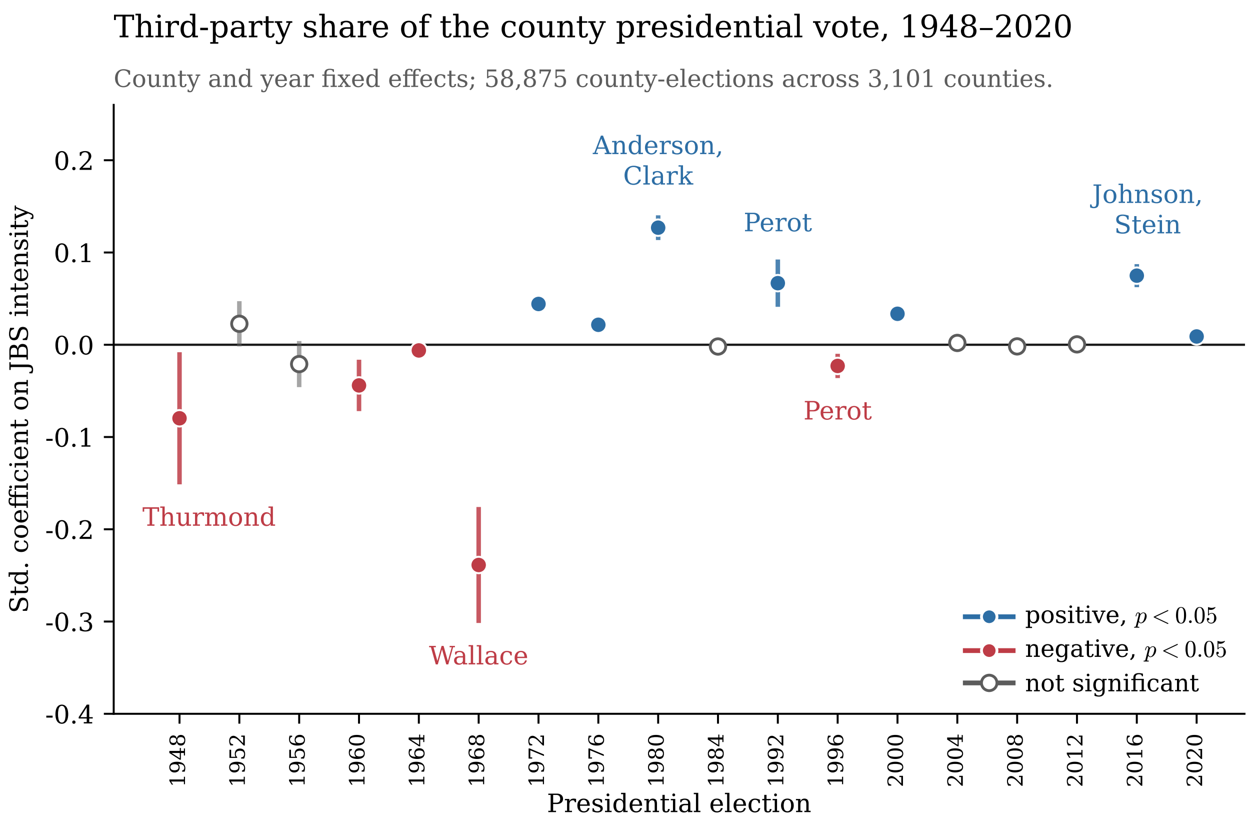


Figure 6: JBS membership and third-party presidential voting, 1948–2020

*Notes.* Coefficients on standardised $\log(1 + \text{JBS members})$ interacted with election year, from a single regression of the standardised third-party share of the county presidential vote on county and year fixed effects. 58,875 county-elections across 3,101 counties and 19 elections; 1988 is the omitted year. Bars are 95% confidence intervals from standard errors clustered by county. Blue marks positive and red negative coefficients significant at 5%; hollow markers are not significant.

## 5.3 Contemporary Attitudes and the Trump Question

The national CES estimates locate a recognizable conservative partisan profile. Nine of 48 outcomes survive familywise correction, including Republican identification, conservative ideology, and three gun-policy positions. None of those five associations survives the matched state-fixed-effects family. The CES evidence therefore describes conservative sorting across states rather than a common within-state county pattern. The fiscal and historical-programme items are less coherent: the identity of the surviving spending item changes across geographic specifications, while the sovereignty, trade, immigration, and social-policy items do not form a stable programme.

Nationscape supplies the narrower within-state result. Respondents in JBS-intensive districts are 0.71 percentage points less likely to be registered within states, but among Democratic or Republican primary intenders they are 1.19 points more likely to select the Republican primary. Whether respondents had voted or intended to vote is null. These estimates imply partisan sorting rather than generalized engagement.

Neither survey isolates a distinctive Trump affinity. CES estimates among all respondents, prior Romney voters, and prior Obama voters fail familywise correction nationally and within states; Nationscape Trump favorability and approval are also null at both scales. Table 4 places the selected national and state-fixed-effects estimates side by side, while Appendix Table A1 reports every outcome in the two survey families. The resident-weighted county vote-shift result below therefore should not be read as an individual-level Trump evaluation.

Table 4: Selected CES and Nationscape estimates: national and state fixed effects

| | National | | State fixed effects | | |
|---|---|---|---|---|---|
| Outcome | $\beta$ | RW $p$ | $\beta$ | RW $p$ | $N$ |
| *Panel A. CES 2006–2020* | | | | | |
| Party identification (high = Rep.)$^{\dagger}$ | 0.033*** | 0.002 | 0.018* | 0.585 | 425,038 |
| | (0.008) | | (0.008) | | |
| Ideology (high = conservative)$^{\dagger}$ | 0.026*** | 0.002 | 0.013~ | 0.820 | 408,990 |
| | (0.006) | | (0.007) | | |
| Opposes banning assault rifles | 2.102*** | <0.001 | 1.151** | 0.118 | 273,237 |
| | (0.394) | | (0.394) | | |
| Trump 2016 among Clinton/Trump voters | 1.015* | 0.661 | 0.492 | 1.000 | 131,821 |
| | (0.504) | | (0.518) | | |
| *Panel B. Nationscape 2019–2021* | | | | | |
| Registered to vote | −0.882*** | <0.001 | −0.711*** | 0.014 | 424,098 |
| | (0.173) | | (0.214) | | |
| Republican rather than Democratic primary intention | 1.115*** | 0.009 | 1.194** | 0.043 | 240,990 |
| | (0.333) | | (0.412) | | |
| Has voted or intends to vote in 2020 | −0.062 | 0.992 | −0.268~ | 0.537 | 326,272 |
| | (0.142) | | (0.156) | | |
| Trump approval$^{\dagger}$ | −0.001 | 0.992 | 0.001 | 0.848 | 408,842 |
| | (0.007) | | (0.007) | | |

*Notes.* These eight rows are theory-relevant contrasts selected for the main-text summary; Appendix Table A1 reports every outcome in both complete families. Survey-weighted estimates are per geographic standard deviation of $\log(1 + \text{JBS members})$; standard errors clustered by county (CES) or congressional district (Nationscape) are in parentheses. Binary outcomes are in pp; $^{\dagger}$marks standardised multi-point scales; Trump approval is oriented so higher values indicate greater approval. State-fixed-effects models use the same outcome-specific samples, weights, controls, time effects, and geographic clusters as the national models. RW $p$ is the Romano–Wolf step-down familywise value from 4,999 shared cluster-influence Rademacher draws within the 48-outcome CES or 21-outcome Nationscape family. Stars use the conventional cluster-robust test: $^{\sim}p < 0.10$; $^{*}p < 0.05$; $^{**}p < 0.01$; $^{***}p < 0.001$.

## 5.4 Bounds and Limitations

The ANES provides a further bound rather than a separate positive result. General anti-statism, racial resentment in the post-snapshot period, and the Perot and Buchanan thermometers fail familywise correction. A few individual items survive, but several related associations are already present before the 1987 membership snapshot. Because the Society had existed since 1958, those earlier estimates are not no-treatment placebos; they show instead that a stock measured in 1987 cannot date when the political geography emerged. Appendix Table A3 reports the complete weighted and unweighted families beside the available pre-snapshot comparisons.

The analysis is correlational throughout. The 1948 Thurmond result indicates that part of the measured geography predates the organization, and the national/state contrast shows that many later associations lie across rather than within states. FEC records are transactions rather than unique donors, the itemization threshold and county-mapping coverage change across cycles, and the estimates attenuate with county affluence. Survey weights target different populations, outcome missingness changes samples, and the post-2000 education control is carried forward from its latest available vintage. These limitations bound the claims without changing the central descriptive result: the rolls align most consistently with one strand of Republican partisan and primary politics.

# 6 Republican Alignment and the Limits of a Populist Legacy

The preceding results imply a bounded contemporary question. I revisit three published county-level studies—January 6 defendants (Pape, Larson, and Ruby 2024), Trump's 2016 vote-share gain over Romney (Broz, Frieden, and Weymouth 2021), and right-wing terrorism (Nemeth and Hansen 2022)—and examine the 2020 certification split among Republican districts. These are descriptive tests of where the 1987 membership geography does and does not align with later outcomes. Full replication, geographic-alignment, exposure, weighting, and influence checks appear in Appendix Tables A6–A13.

## 6.1 January 6 Defendants: Counts and Incidence

The replicated Pape, Larson, and Ruby (2024) benchmark closely reproduces the published coefficients. In its linear-population count specification, a one-standard-deviation increase in logged JBS membership is associated with 50% more defendants (IRR = 1.50, $p < 0.001$). That model asks which counties produce more defendants after a linear population adjustment; it does not estimate defendants per resident.

Population scale changes the result. When log population is estimated freely, its elasticity is 1.053 (SE = 0.071) and is not distinguishable from proportional scaling. I therefore use log 2020 population as an offset for the incidence question. In that specification, the JBS estimate is close to one and null (IRR = 0.96, $p = 0.45$); contemporary population scaling and an any-JBS indicator yield the same conclusion. JBS geography predicts defendant volume in the published benchmark but not defendants per resident. Appendix Table A12 reports the two estimands and the supporting population tests.

## 6.2 Electoral Conversion

The Broz, Frieden, and Weymouth (2021) replication produces a resident-weighted rather than an average-county result. In the population-weighted specification, JBS intensity predicts a smaller 2012–2016 Republican vote-share gain ($\beta = -0.91$, SE $= 0.16$), and the estimate remains negative after controlling for Romney's 2012 share. The unweighted estimate for the average county is near zero ($\beta = -0.09$, $p = 0.31$). The rolls therefore locate populous counties that shifted relatively little toward Trump, not a general individual-level affinity or aversion. Appendix Table A10 reports the weighting, exposure, and baseline-vote checks.

## 6.3 Right-Wing Terrorism

The terrorism replication provides no detectable JBS association ($\beta = -0.02$, $p = 0.91$), and the conclusion is unchanged in the pre- and post-1987 windows. The exercise is necessarily limited: the outcome contains only 192 events across 133,539 county-years, and pooled logit with county-clustered errors only approximates the original mixed-effects model. Even so, it offers no support for treating JBS geography as a general index of contemporary right-wing violence (Appendix Table A11).

## 6.4 Partisan Geography and Certification

Republican-held districts contain substantially more JBS membership than Democratic-held districts: population-scaled means are 17.92 versus 10.32 records per 100,000, and the population-offset IRR is 1.74 ($p < 0.001$). Among Republican districts, however, membership does not distinguish certification objectors from certifiers; the corresponding IRR is 0.86 ($p = 0.241$). The rolls align with Republican seat geography, not with which Republican representatives objected to certification (Appendix Table A13).

A contemporary review links Bircher opposition to fluoridation and promotion of laetrile as a cancer treatment with present-day ivermectin enthusiasm (Green 2023). This motivates a county comparison, not a claim of continuity or transmission. National CMS files (Centers for Medicare & Medicaid Services 2026; Centers for Medicare & Medicaid Services, Office of Enterprise Data and Analytics 2024) yield a null broad estimate (0.028, SE $= 0.051$) and a null generic–topical difference (wild-bootstrap $p = 0.570$). CMS suppresses provider–drug rows with ten or fewer claims and locates claims at the provider; in 2021, any ivermectin row appears in 5.6% of the smallest-market decile versus 92.2% of the largest. In the top half by 2019 Part D claims, the generic–topical contrast changes across specifications (wild-bootstrap $p = 0.024$ with baseline controls and 0.058 with expanded controls); fixed-weight and untransformed estimates are null, and the minimum Benjamini–Hochberg $q$ across 30 threshold tests is 0.094. The evidence does not establish continuity, intellectual lineage, or resident ivermectin use. Appendix Table A5 and Figure A4 report the details.

# 7 Conclusion

This paper turns 45,188 archival membership records into an individual-record, geocoded map of the John Birch Society. The map reveals a specific strand of the American right. Outside the Deep South, later JBS presence aligns with the Goldwater-era Republican swing; within the Deep South, the relationship reverses. The denominational and third-party results point in the same direction: the rolls locate an organized, anti-communist, free-market, and often suburban network rather than generic conservative or Wallace-style politics.

The later record is best described as partisan absorption rather than organizational survival. Nationally, JBS-intensive places exhibit selective primary participation, conservative partisan attitudes, gun-policy conservatism, and itemized federal-receipt activity. Most of those associations lie across states. Within states, the durable evidence narrows to 1980 receipt activity and, three decades later, lower registration coupled with Republican-primary sorting. The pre-founding Thurmond result further shows that the Society entered a political geography it did not wholly create.

The contemporary applications reinforce that boundary. Survey respondents do not exhibit a distinctive Trump affinity; the resident-weighted county vote-shift estimate is absent for the average county; JBS geography predicts January 6 defendant volume but not per-resident incidence; and the terrorism and certification-objector comparisons are null. The rolls therefore do not provide a general map of contemporary populism or political violence.

These alignments remain descriptive. Establishing causal persistence will require variation in the timing and geography of JBS organizing, such as field-staff assignments, chapter coordinators, or organizing drives documented in the *JBS Bulletin*. Methodologically, the digitization pipeline shows how structured archival records can become traceable political data without treating OCR as a black box, while the January 6 comparison shows why count outcomes require an explicit choice between volume and incidence. The resulting data provide a reusable foundation for studying how this organized strand of the American right was transformed, absorbed, or not straightforwardly inherited by later politics.

# Data Availability and Ethics

The published paper redacts personal identifiers from source images. Public replication materials will release county and district aggregates, code, and crosswalks sufficient to reproduce the analyses, but not named individual-level membership records. Individual-level named data should be restricted to controlled replication use, subject to archival permissions and an IRB or institutional determination for secondary use of sensitive archival records.

All other data used here are public. Section 5 draws on county presidential returns, 1868–2020 (Algara and Amlani 2021); individual contributions and the committee master file from the Federal Election Commission (Federal Election Commission 2026); the Cumulative Cooperative Election Study and its policy-preferences companion (Kuriwaki 2026; Ansolabehere, Schaffner, and Luks 2021); the Democracy Fund + UCLA Nationscape surveys (Tausanovitch and Vavreck 2021); and the ANES Time Series Cumulative Data File (American National Election Studies 2022). County and district religious composition comes from the Association of Religion Data Archives' longitudinal Religious Congregations and

Membership File (Grammich et al. 2018), whose merge rules and limits are documented by Bacon, Finke, and Jones (2018); that file aggregates some county units, and the aggregation is carried through to the analysis rather than undone. County per-capita personal income is from the Bureau of Economic Analysis (U.S. Bureau of Economic Analysis 2025), county educational attainment from IPUMS NHGIS (Schroeder et al. 2026), and the ZCTA–county and ZCTA–congressional-district crosswalks from the Census Bureau (U.S. Census Bureau 2019). Tables and figures are generated directly from the estimation output rather than transcribed; the replication package includes the generating scripts.

The exploratory claims analysis uses the annual Medicare Part D Prescribers by Provider and Drug files and the Provider PUF from the Centers for Medicare & Medicaid Services (Centers for Medicare & Medicaid Services 2026; Centers for Medicare & Medicaid Services, Office of Enterprise Data and Analytics 2024). For provider ZIP codes that match a five-digit 2020 ZCTA, I assign the ZCTA to the county containing the largest share of its land area using the 2020 ZCTA–county relationship file; unmatched records do not enter the county totals (U.S. Census Bureau 2020). The classifications of Soolantra and Sklice as topical products follow their DailyMed labels (U.S. National Library of Medicine 2024b; U.S. National Library of Medicine 2024a).

# 8 Appendix

The appendix proceeds from data construction to empirical results. Sections 8.1–8.4 document archival access, scanning, model implementation, and verification. Sections 8.5 and 8.6 report supplementary descriptive statistics, full model estimates, and robustness checks.

## 8.1 Archival Access and Scanning Workflow

The membership rolls consist of continuous-feed dot-matrix printouts, making them physically legible but poorly suited to direct OCR. The pages are regular enough to support model-based extraction, but the combination of dot-matrix characters, faint print, page curvature, and long narrow text lines made off-the-shelf OCR unreliable.

Scanning required coordination with library staff because the records could not be removed from the archive, archive appointments had to be arranged well in advance, and scanner access was sometimes limited. The first collection pass took 20 days, from June 5 to June 25, 2024. The workflow unfolded over two years: research assistants corrected and verified lines during the 2024–25 academic year, and final validation and empirical integration continued through spring 2026. The conceptual framework—modular pipeline, fine-tuned detection, and human-in-the-loop labeling—came from Dell (2025)'s body of work. Dell's advice about matching object-detection anchors to target geometry shaped the line-detection stage: long text lines required radically different anchors than the natural objects these models are pretrained on.

## 8.2 Pipeline Implementation Details

Table 5 provides the model choices, training data, hyperparameters, metrics, and training time for each stage of the pipeline. Layout detection produced page-level crops, line detection produced line-level crops, OCR produced line-level predictions, and parsing produced structured records. Figure 7 shows representative source-image examples for the layout-detection, line-detection, and OCR stages of the workflow.

Table 5: Digitization pipeline implementation details

| Stage | Model | Training data | Hyperparameters, metric, and time |
|---|---|---|---|
| Layout Detection | YOLOv8n | 1,314 training crops (146 val.) | *Hyperparameters:* epochs: 100; optimizer: AdamW. *Metric:* mAP50: 99.5%; mAP50–95: 96%. *Time:* 10 days, including labeling and training. |
| Line Detection | Faster R-CNN (ResNeXt-101-32x8d-FPN) | 7,732 training crops | *Hyperparameters:* iterations: 224,700; lr: 1e-4; batch: 8; anchors: [.02-.04]. *Metric:* Classification accuracy: 96.7%. *Time:* 7 hours training. |
| OCR | TrOCR (base-printed) | 74,517 training lines (8,280 val.) | *Hyperparameters:* epochs: 60; lr: 4e-5; batch: 16; beams: 4. *Metric:* CER: 0.32%. *Time:* 21 hours training. |

*Notes:* All training was conducted on two NVIDIA GPUs with 40 GB of memory on Boston University's Shared Computing Cluster. Line segmentation used Detectron2 with a COCO-pretrained backbone. OCR used HuggingFace Transformers with Accelerate for multi-GPU training.

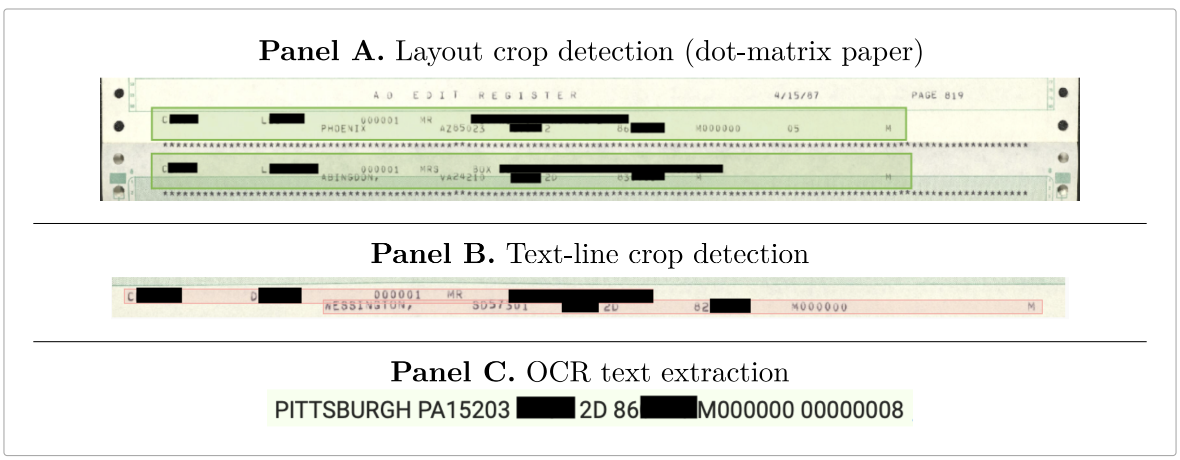


Figure 7: Representative redacted source-image examples for the digitization workflow. The panels show the visual inputs behind layout detection, line detection, and OCR, complementing the schematic pipeline in Figure 1. Black boxes indicate redactions of names, street addresses, and box numbers added for publication; city, state, ZIP code, chapter markers, and administrative codes are reproduced as they appear in the source scans.

## 8.3 Deskewing, Hashing, and Duplicate Handling

Several preprocessing experiments produced useful lessons. I initially tried deskewing because slight page rotation made line detection harder. Deskewing helped some images, but it also changed pixel coordinates and created bookkeeping problems across layout labels, line crops, and source-image links.

Image hashing—computing a perceptual fingerprint for each file—helped recover mappings when preprocessing changed file names or directory structure, but the added maintenance cost outweighed the accuracy gain. As the training set grew, the line detector became robust enough to residual skew that I stopped deskewing and rehashing as routine steps.

## 8.4 Research Assistant Workflow and Time Costs

The project required approximately 300 research-assistant hours across two research assistants over eight months. Manual transcription of 45,188 two-line records would have required substantially more labor, conservatively 1,500 to 2,000 hours at realistic transcription speeds. The largest bottleneck was line segmentation, because correcting bounding boxes around long narrow text strips requires pixel-level precision.

## 8.5 Supplementary Descriptive Tables

Table 6 reports membership records by salutation category and geographic coverage. Table 7 compares counties with JBS members, counties with January 6 defendants, and all counties. The tables supplement the descriptive discussion in Section 4.

Table 6: Membership records by salutation category and geographic coverage

| | Count | % |
|---|---:|---:|
| Male | 26,394 | 58.4 |
| Female | 16,385 | 36.3 |
| Couple | 638 | 1.4 |
| Professional | 1,271 | 2.8 |
| Other | 500 | 1.1 |
| Total records | 45,188 | 100.0 |
| Counties covered | 2,456 | of 3,141 |
| States covered | 50 | + DC |

*Notes:* Unit is a membership record, not necessarily a unique individual. Gender is inferred from salutation fields (Mr, Mrs, Ms, Miss, and related variants). "Professional" denotes records with MD, DDS, DVM, or similar title but no gendered salutation. "Couple" denotes joint spousal records (Mr & Mrs). Membership rolls date from mid-1987. County coverage includes only records matched through the ZCTA crosswalk and excludes geographies outside the analysis universe; see Section 4.

Table 7: Descriptive comparison of counties with JBS members and counties with January 6 defendants

| | JBS counties | Defendant counties | All counties |
|---|---|---|---|
| *Key Independent Variables (means)* | | | |
| White pop. decline (%) | 4.42 | 5.62 | 4.15 |
| Mfg employment decline (%) | 8.25 | 12.60 | 8.05 |
| Trump 2020–Romney 2012 vote-share gap (pp) | 4.89 | 1.29 | 5.40 |
| *Demographics* | | | |
| Non-Hispanic white (%) | 74.2 | 69.1 | 74.2 |
| Urban county (%) | 28.9 | 65.9 | 25.7 |
| *Overlap* | | | |
| Counties with both JBS & defendants | 415 of 458 defendant counties (90.6%) | | |
| Avg. defendants, high JBS | 0.645 vs. 0.082 in counties with no JBS | | |
| Spearman $\rho$ | $0.308^{***}$ | | |
| $N$ | 2,456 | 458 | 3,141 |

*Notes:* JBS counties have at least 1 member in the mid-1980s rolls. Defendant counties have at least 1 individual charged by the DOJ for the January 6, 2021, Capitol breach as of April 2023. "High JBS" counties are above the median among counties with any JBS members. $^{***}p < 0.001$.

## 8.6 Supplementary Empirical Tables

The first block documents the complete later-outcome families, their shared inference procedures, and the diagnostics summarized in Section 5. The second reports the full January 6 benchmark, replication checks, population-treatment sensitivity, electoral-conversion and terrorism specifications, and district-level partisan and certification comparisons. The final block documents the exploratory public-claims coda in Section 6, including its outcome definitions, provider-volume restrictions, transformations, exposure scales, provider-structure controls, weighting choices, and inference checks.

### Later-outcome design and inference

Five sources support Section 5, all merged to the rolls at the county or congressional-district level. County presidential returns run from 1948 to 2020 (Algara and Amlani 2021); FEC-classified itemized individual receipts cover 1980, 1992, 1996, and 2012 (Federal Election Commission 2026); the Cumulative Cooperative Election Study supplies validated turnout and policy items for 2006–2020 (Kuriwaki 2026; Ansolabehere, Schaffner, and Luks 2021); Nationscape supplies district-level responses from 2019–2021 (Tausanovitch and Vavreck 2021); and the ANES cumulative file covers 1978–1998 (American National Election Studies 2022).

The FEC outcomes are signed receipt dollars per capita and positive receipt records per capita; a record is not a unique donor. Signed dollars are aggregated before county net amounts are transformed as $\log(1 + \max\{x, 0\})$. In the FEC and CES models, $\log(1 + \text{JBS records})$ is standardized once over unique counties; in Nationscape it is standardized once over unique congressional districts. FEC models include county religious composition (Grammich et al. 2018), contemporaneous log population, South, annual per-capita personal income (U.S. Bureau of Economic Analysis 2025), and bachelor's-degree share (Schroeder et al. 2026). CES models add individual age, education, income, race, gender, and religion, use the cumulative survey weight, and include year fixed effects. Nationscape uses its survey weight, analogous district and individual controls, and weekly-wave fixed effects. Multi-point survey outcomes are standardized using the corresponding survey weights. The third-party event study instead absorbs county and election-year fixed effects. State-fixed-effects estimates retain the same observations, weights, controls, time effects, and geographic clusters as the corresponding national models.

Multiplicity is handled within complete source families fixed before resampling: all 48 CES behavior, Trump-subgroup, and policy outcomes; all 21 retained Nationscape outcomes; and eight aggregate FEC receipt outcomes. Romano–Wolf step-down values use 4,999 shared cluster influence-score multiplier draws with Rademacher weights over a fixed sorted cluster universe and plus-one $p$-values (Romano and Wolf 2005). Sharing draws within each family preserves cross-outcome dependence in the maximum statistic. This is an asymptotic multiplier procedure based on fitted cluster influence scores, not a restricted-residual wild bootstrap. The nineteen candidate-level and candidate-share tests use one joint Holm family; the ANES uses a separate seventeen-outcome resampling family.

Table A1: Every modern-era outcome: national and state-fixed-effects specifications

| Outcome | National specification β | (SE) | RW $p$ | State fixed effects β | (SE) | RW $p$ | $N$ |
|---|---|---|---|---|---|---|---|
| **Panel A. Cumulative CES 2006–2020, by county** | | | | | | | |
| *Behaviour, participation and partisanship* | | | | | | | |
| Validated primary turnout | 0.025*** | (0.004) | <0.001 | −0.001 | (0.003) | 1.000 | 341,618 |
| Validated general-election turnout | 0.008* | (0.003) | 0.450 | 0.002 | (0.003) | 1.000 | 341,607 |
| Primary minus general-election turnout | 0.017*** | (0.004) | <0.001 | −0.003 | (0.003) | 0.999 | 341,606 |
| Registered Republican and validated primary voter | 0.008* | (0.003) | 0.352 | 0.002 | (0.002) | 1.000 | 263,705 |
| Republican registration among D/R primary voters | 0.041*** | (0.009) | <0.001 | 0.016* | (0.008) | 0.693 | 35,002 |
| Interest in politics | −0.003 | (0.005) | 1.000 | −0.003 | (0.006) | 1.000 | 429,919 |
| Party identification (high = Republican) | 0.033*** | (0.008) | 0.002 | 0.018* | (0.008) | 0.585 | 425,038 |
| Ideology (high = conservative) | 0.026*** | (0.006) | 0.002 | 0.013~ | (0.007) | 0.820 | 408,990 |
| Republican presidential vote among D/R voters | 0.012** | (0.004) | 0.084 | 0.005 | (0.004) | 0.998 | 300,543 |
| Republican U.S. House vote among D/R voters | 0.016** | (0.005) | 0.072 | 0.012* | (0.005) | 0.541 | 218,899 |
| Republican U.S. Senate vote among D/R voters | 0.008 | (0.006) | 0.951 | 0.004 | (0.004) | 1.000 | 148,084 |
| Republican gubernatorial vote among D/R voters | 0.016** | (0.006) | 0.198 | 0.008 | (0.005) | 0.982 | 96,995 |
| Presidential approval | −0.002 | (0.005) | 1.000 | 0.002 | (0.006) | 1.000 | 427,556 |
| Retrospective economic evaluation | 0.005 | (0.005) | 0.997 | 0.001 | (0.005) | 1.000 | 430,053 |
| Born-again Christian | 0.001 | (0.003) | 1.000 | −0.003 | (0.003) | 0.999 | 431,622 |
| *Trump-subgroup contrasts* | | | | | | | |
| Trump 2016 among Clinton/Trump voters | 0.010* | (0.005) | 0.661 | 0.005 | (0.005) | 1.000 | 131,821 |
| Trump 2016 among 2012 Romney voters | −0.003 | (0.004) | 1.000 | −0.006 | (0.004) | 0.986 | 12,744 |
| Trump 2016 among 2012 Obama voters | −0.011~ | (0.006) | 0.728 | −0.010 | (0.007) | 0.975 | 18,960 |
| *Sovereignty and military policy* | | | | | | | |
| Oppose U.S. force to uphold UN law | 0.001 | (0.003) | 1.000 | 0.001 | (0.003) | 1.000 | 296,256 |
| Oppose using force to protect allies | −0.006* | (0.003) | 0.358 | −0.003 | (0.003) | 1.000 | 296,256 |
| Oppose using force to spread democracy | 0.001 | (0.002) | 1.000 | 0.002 | (0.003) | 1.000 | 296,256 |
| Oppose using force to stop genocide | −0.003 | (0.003) | 0.987 | 0.001 | (0.003) | 1.000 | 296,256 |
| Use force to secure oil supplies | −0.002 | (0.003) | 1.000 | 0.002 | (0.003) | 1.000 | 296,256 |
| Use force to destroy a terrorist camp | 0.004 | (0.002) | 0.915 | 0.003 | (0.003) | 0.999 | 296,256 |
| *Trade* | | | | | | | |
| Restrict trade with China | 0.003 | (0.004) | 0.999 | 0.004 | (0.004) | 1.000 | 123,381 |
| Oppose tariffs including Canada/Mexico | 0.004 | (0.005) | 0.999 | 0.000 | (0.005) | 1.000 | 123,191 |
| *Guns* | | | | | | | |

*Continued on next page*

*Appendix Table A1 continued*

| | National specification | | | State fixed effects | | | |
|---|---|---|---|---|---|---|---|
| Outcome | $\beta$ | (SE) | RW $p$ | $\beta$ | (SE) | RW $p$ | $N$ |
| Oppose banning assault rifles | 0.021*** | (0.004) | <0.001 | 0.012** | (0.004) | 0.118 | 273,237 |
| Oppose universal background checks | 0.011*** | (0.003) | 0.002 | 0.003 | (0.003) | 0.999 | 219,115 |
| Support easing concealed-carry permits | 0.015*** | (0.004) | 0.002 | 0.010* | (0.004) | 0.349 | 273,466 |
| Support prohibiting publication of owner names | 0.010** | (0.004) | 0.116 | 0.007~ | (0.004) | 0.808 | 204,391 |
| *Spending: means-tested* | | | | | | | |
| Cut welfare spending | 0.024** | (0.008) | 0.096 | 0.027*** | (0.008) | 0.025 | 183,231 |
| *Spending: universal* | | | | | | | |
| Cut education spending | 0.010 | (0.008) | 0.987 | 0.017* | (0.008) | 0.723 | 183,136 |
| Cut health-care spending | 0.027*** | (0.008) | 0.019 | 0.022** | (0.008) | 0.162 | 183,217 |
| Cut infrastructure spending | 0.024* | (0.009) | 0.246 | 0.024** | (0.007) | 0.053 | 183,058 |
| Cut police spending | −0.005 | (0.008) | 1.000 | 0.003 | (0.007) | 1.000 | 183,026 |
| Balance budget by cutting rather than taxing | 0.011 | (0.007) | 0.915 | 0.018* | (0.008) | 0.474 | 269,761 |
| *Immigration* | | | | | | | |
| Build a border wall | 0.008~ | (0.004) | 0.837 | 0.003 | (0.005) | 1.000 | 123,717 |
| Deport undocumented immigrants | 0.002 | (0.004) | 1.000 | 0.004 | (0.005) | 1.000 | 135,924 |
| Oppose a path to legal status | 0.007* | (0.003) | 0.512 | 0.004 | (0.003) | 0.987 | 343,595 |
| Police may question immigration status | −0.001 | (0.004) | 1.000 | −0.008* | (0.004) | 0.674 | 206,694 |
| Deny public services to undocumented | 0.004 | (0.006) | 1.000 | −0.008 | (0.006) | 0.996 | 62,308 |
| *Social* | | | | | | | |
| Oppose always allowing abortion | 0.008~ | (0.004) | 0.722 | 0.002 | (0.004) | 1.000 | 259,354 |
| Prohibit all abortion | 0.001 | (0.004) | 1.000 | −0.004 | (0.004) | 0.999 | 210,091 |
| Oppose legalising same-sex marriage | 0.006 | (0.004) | 0.933 | 0.002 | (0.004) | 1.000 | 180,974 |
| Opposition to affirmative action (1-4) | 0.011 | (0.007) | 0.942 | 0.008 | (0.007) | 1.000 | 220,849 |
| *Environment* | | | | | | | |
| Oppose regulating carbon emissions | 0.011** | (0.004) | 0.072 | 0.002 | (0.004) | 1.000 | 251,843 |
| Oppose requiring renewable energy | 0.008* | (0.004) | 0.538 | 0.001 | (0.004) | 1.000 | 252,042 |
| Prioritise jobs over the environment | 0.000 | (0.009) | 1.000 | −0.002 | (0.009) | 1.000 | 149,152 |
| **Panel B. 2019–21 national survey (Nationscape), by congressional district** | | | | | | | |
| Registered to vote | −0.009*** | (0.002) | <0.001 | −0.007*** | (0.002) | 0.014 | 424,098 |
| Has voted or intends to vote in 2020 | −0.001 | (0.001) | 0.992 | −0.003~ | (0.002) | 0.537 | 326,272 |
| Republican rather than Democratic primary intention | 0.011*** | (0.003) | 0.009 | 0.012** | (0.004) | 0.043 | 240,990 |
| Trump rather than Clinton vote in 2016 | 0.004 | (0.004) | 0.839 | 0.007 | (0.004) | 0.551 | 281,702 |
| Party identification (high = Republican) | 0.016* | (0.006) | 0.105 | 0.019** | (0.007) | 0.088 | 283,932 |

*Continued on next page*

*Appendix Table A1 continued*

| | National specification | | | State fixed effects | | | |
|---|---|---|---|---|---|---|---|
| Outcome | $\beta$ | (SE) | RW $p$ | $\beta$ | (SE) | RW $p$ | $N$ |
| Ideology (high = conservative) | 0.015** | (0.005) | 0.061 | 0.012~ | (0.007) | 0.517 | 388,845 |
| Interest in politics | −0.010** | (0.004) | 0.079 | −0.012* | (0.005) | 0.138 | 432,740 |
| Approval of Trump | −0.001 | (0.007) | 0.992 | 0.001 | (0.007) | 0.848 | 408,842 |
| Favorability toward Trump | −0.002 | (0.007) | 0.992 | 0.005 | (0.007) | 0.845 | 412,402 |
| Coldness toward Obama | 0.010 | (0.006) | 0.551 | 0.016* | (0.008) | 0.325 | 408,270 |
| Favorability toward the police | −0.007~ | (0.004) | 0.551 | −0.007 | (0.005) | 0.620 | 389,286 |
| Coldness toward labor unions | 0.016** | (0.005) | 0.026 | 0.011~ | (0.006) | 0.537 | 332,109 |
| Coldness toward socialists | 0.018* | (0.008) | 0.150 | 0.025** | (0.009) | 0.041 | 326,966 |
| Favorability toward Christians | −0.002 | (0.009) | 0.992 | 0.012 | (0.011) | 0.736 | 43,010 |
| Coldness toward undocumented immigrants | 0.005 | (0.006) | 0.898 | 0.021** | (0.007) | 0.036 | 371,892 |
| Favorability toward Republicans | 0.001 | (0.006) | 0.992 | 0.006 | (0.007) | 0.843 | 387,814 |
| Coldness toward Democrats | 0.013* | (0.006) | 0.264 | 0.019* | (0.007) | 0.108 | 389,236 |
| Gets news from Fox | −0.006* | (0.003) | 0.237 | −0.004 | (0.003) | 0.593 | 425,078 |
| Gets news from NPR | 0.004* | (0.002) | 0.223 | 0.003 | (0.002) | 0.730 | 425,078 |
| Gets news from AM talk radio | −0.001 | (0.002) | 0.992 | −0.002 | (0.003) | 0.845 | 425,078 |
| Gets news from a local newspaper | −0.006 | (0.004) | 0.551 | −0.003 | (0.004) | 0.845 | 425,078 |
| **Panel C. FEC-classified itemized individual receipts, county × cycle** | | | | | | | |
| *Receipt dollars per capita* | | | | | | | |
| Receipt dollars p.c., 1980 | 0.112*** | (0.023) | <0.001 | 0.106*** | (0.026) | <0.001 | 3,084 |
| Receipt dollars p.c., 1992 | 0.063** | (0.021) | 0.007 | 0.044~ | (0.023) | 0.143 | 3,088 |
| Receipt dollars p.c., 1996 | 0.096*** | (0.022) | <0.001 | 0.054* | (0.023) | 0.069 | 3,088 |
| Receipt dollars p.c., 2012 | 0.025 | (0.018) | 0.379 | 0.026 | (0.019) | 0.381 | 3,088 |
| *Positive receipt records per capita* | | | | | | | |
| Positive receipt records p.c., 1980 | 0.091*** | (0.027) | 0.001 | 0.089** | (0.033) | 0.027 | 3,084 |
| Positive receipt records p.c., 1992 | 0.034 | (0.027) | 0.379 | 0.016 | (0.025) | 0.771 | 3,088 |
| Positive receipt records p.c., 1996 | 0.087*** | (0.026) | 0.001 | 0.049* | (0.023) | 0.119 | 3,088 |
| Positive receipt records p.c., 2012 | −0.008 | (0.023) | 0.749 | 0.003 | (0.021) | 0.877 | 3,088 |

*Notes.* Binary outcomes are in probability units; multi-point and transformed FEC outcomes are standardised. Standard errors cluster by county or district. Both columns retain, where applicable, the weights, controls, time effects, and outcome-specific samples of the main models; the right-hand columns add state fixed effects. RW $p$ uses Romano–Wolf step-down with 4,999 shared cluster-influence Rademacher draws and plus-one values. Stars are the conventional cluster-robust test: $^{\sim}p < 0.10$; $^{*}p < 0.05$; $^{**}p < 0.01$; $^{***}p < 0.001$.

### Additional movement-conservatism diagnostics

Figure A1 shows the sensitivity of the FEC estimates to measured county affluence. Adding county income and education reduces the mean national dollar coefficient from 0.181 to 0.074, a 59% attenuation, and leaves both 2012 FEC outcomes null. In the national CES specification, adding the same geographic controls barely changes primary turnout (2.51 to 2.52 percentage points) or the four gun-policy coefficients. The comparison isolates sensitivity to observed affluence; it does not turn the remaining associations into causal effects.

Figure A2 decomposes the national CES turnout coefficients by election year. The primary coefficient exceeds the general-election coefficient in every available year. Primary turnout averages 3.35 percentage points in 2008–2014 and 1.56 points in 2016–2020; the corresponding general-election averages are 1.38 and 0.07 points. The annual primary-minus-general contrast is individually significant in 2010, 2012, 2014, 2018, and 2020, but not in 2008 or 2016. Because the pooled contrast vanishes with state fixed effects, the repetition documents a cross-state alignment rather than within-state persistence.

Candidate receipt activity is identified using official cycle-specific candidate identifiers and principal or authorized presidential-committee status. For 2012, the construction also requires the official candidate–committee linkage with matching candidate and FEC election years. Because those linkage files begin in 1999–2000, the earlier cycles rely on the candidate and committee master files. Appendix Table A4 reports all nineteen candidate-level and candidate-share tests.

The CES born-again indicator is null, but it measures a different religious margin from the denominational census in Section 4.4. Across 1,293 counties with at least fifty CES respondents, the born-again share correlates 0.77 with evangelical adherence and 0.71 with Southern Baptist adherence, compared with −0.12 for Missouri Synod and −0.14 for Latter-day Saints adherence. A separate top-cluster audit removes, for each outcome, the county or district with the largest absolute coefficient-score contribution and repeats the national familywise adjustment. Eight of nine CES survivors, two of three Nationscape survivors, and all five FEC survivors remain. The two losses are health-care spending after removing New York County ($p_{RW} = 0.074$) and labor-union coldness after removing New York's 10th congressional district ($p_{RW} = 0.077$); neither carries the paper's interpretation.

Figure A3 reports the CES Trump-subgroup estimates. The all-respondent coefficient is 1.02 percentage points but fails the 48-outcome correction ($p_{RW} = 0.661$); conditional estimates among prior Romney and Obama voters and the corresponding state-fixed-effects estimates are also null. Nationscape Trump favorability and approval are likewise null at both geographic scales.

### Measurement limits of the later-outcome data

The FEC source is a transaction-level bulk snapshot. The analysis follows the Commission's itemized-individual transaction-type classification and preserves every distinct transaction record. That classification is not a pure natural-person measure, and the available fields do not permit a complete reconstruction of amendment chains, so superseded filing records may remain. The itemization threshold is 500 in 1980 and 200 in the later cycles. Exact-ZCTA county allocation retains 86.75%, 90.77%, 89.38%, and 95.42% of signed dollars in 1980, 1992, 1996, and 2012, respectively.

The FEC estimates depend materially on affluence controls. Per-capita income is annual, but the county bachelor's-degree share is observed for 1980, 1990, and 2000 and then carried forward after 2000 across the CES and Nationscape windows. Survey weights target different populations across sources, and outcome-specific missingness changes the sample reported in each row. The ANES estimates are period- and weight-sensitive; Appendix Table A3 reports the complete post-snapshot family beside the available pre-snapshot comparisons.

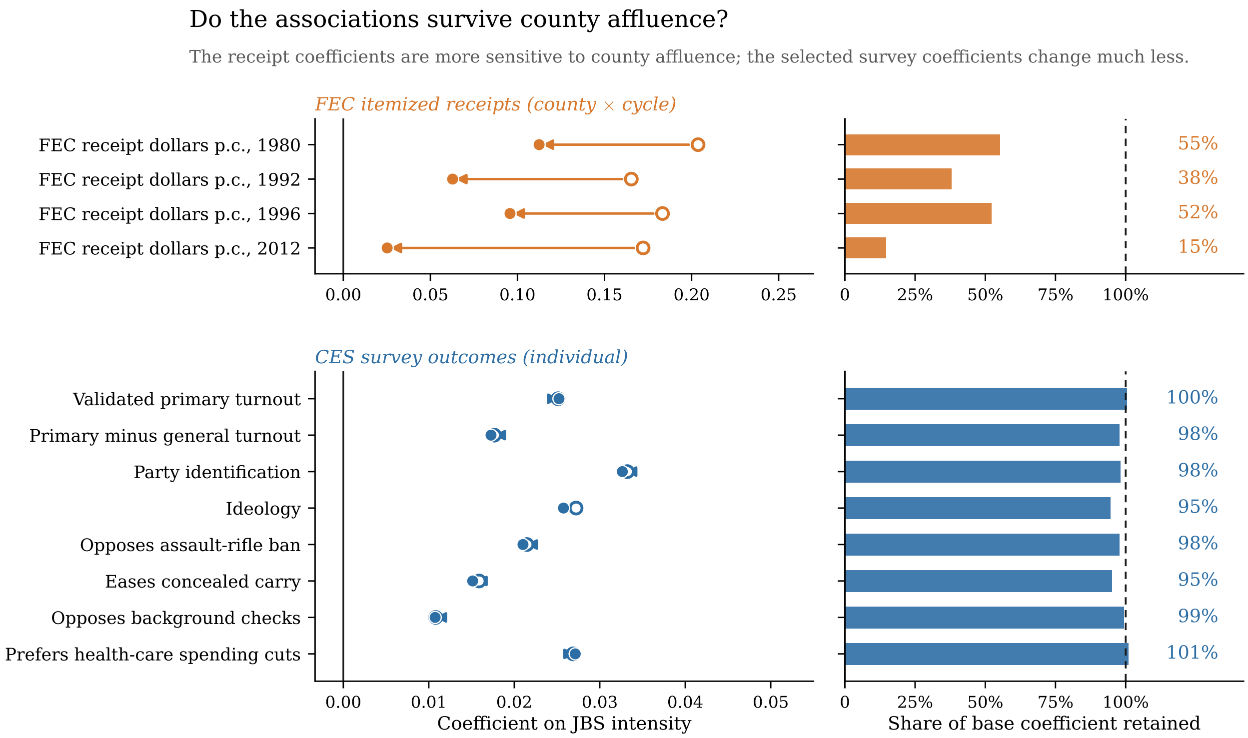


Figure A1: Do the associations survive county income and education?

○ Religion, population, South ● + county income and education

*Notes.* The hollow and filled markers follow the key above. The added controls are BEA per-capita personal income (logged) and the NHGIS bachelor's-degree share. Within each row both specifications are fitted on identical observations. The right-hand panels express the controlled coefficient as a share of the uncontrolled one. FEC and CES outcomes are drawn on separate coefficient scales.

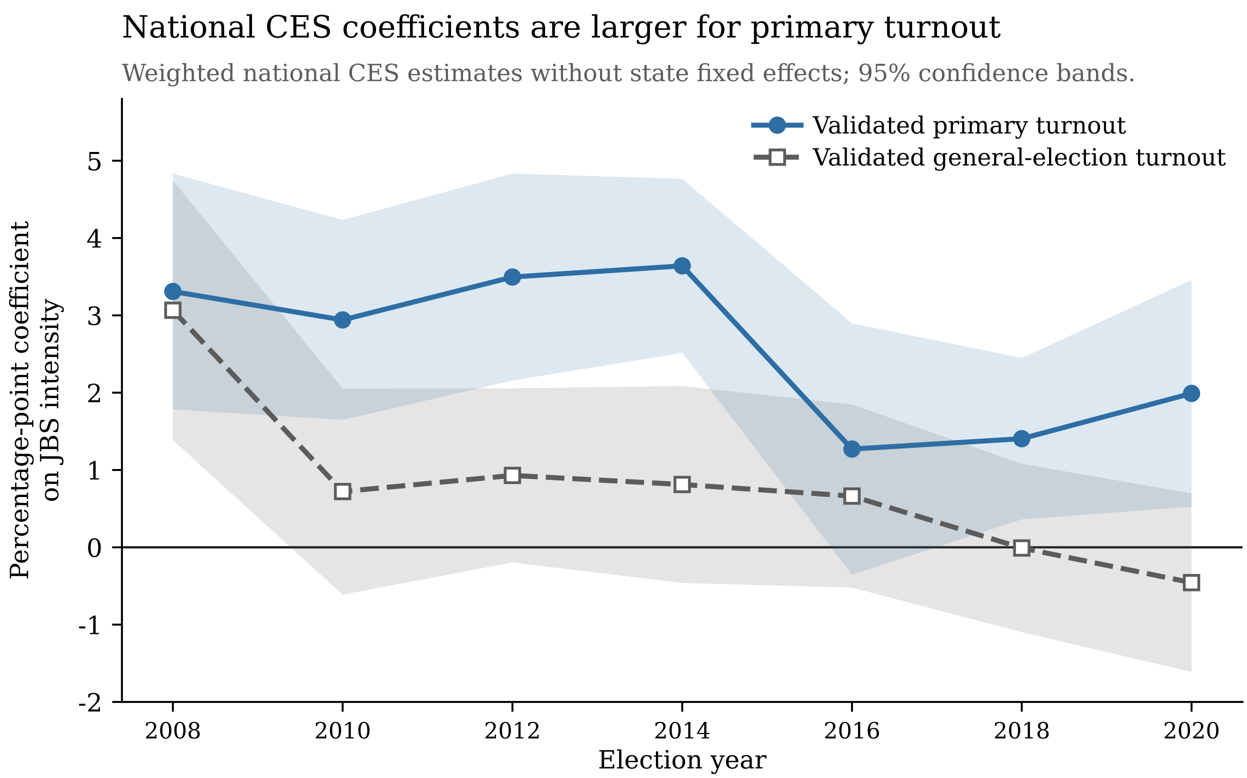


Figure A2: Validated primary and general-election turnout in JBS counties, CES 2008–2020

*Notes.* Separate national survey-weighted regressions by election year, each with the control set of Table 3. Shaded bands are 95% confidence intervals from standard errors clustered by county. Both validated outcomes are binary and shown in percentage points. Appendix Table A1 reports the pooled national and state-fixed-effects estimates.

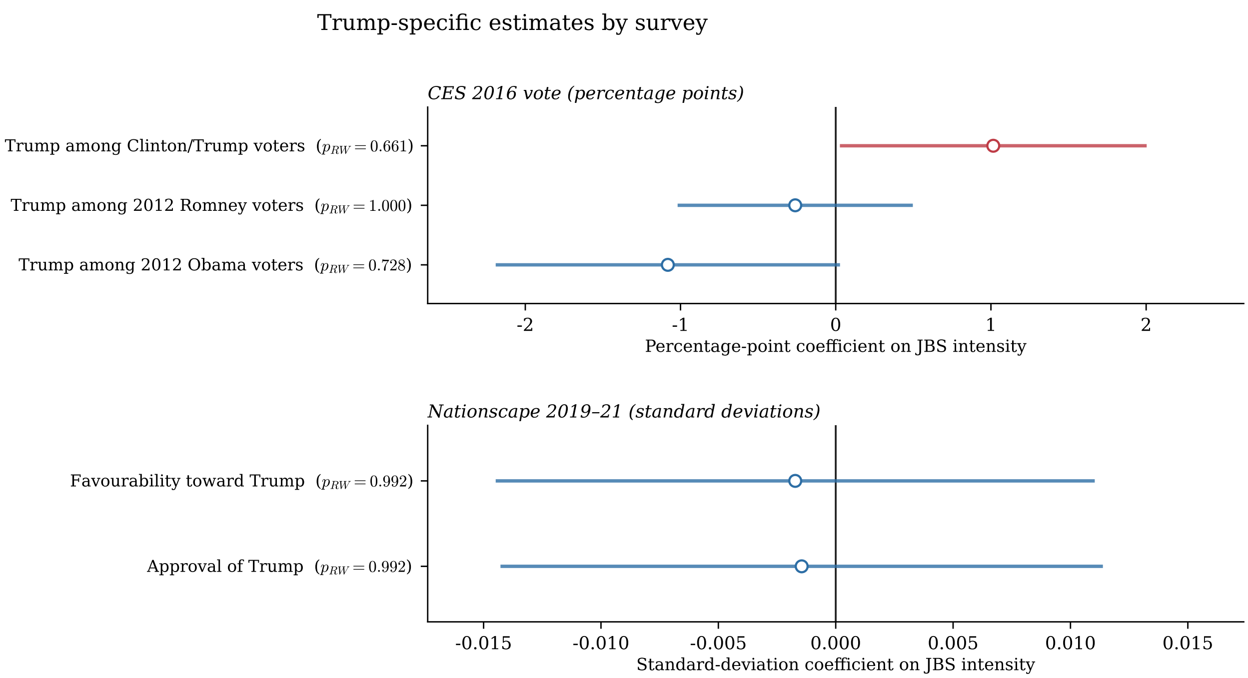


Figure A3: Trump-specific alignment in the CES and Nationscape

*Notes.* Bars are 95% confidence intervals. Hollow markers denote estimates that do not survive Romano–Wolf correction within the 48-outcome CES or 21-outcome Nationscape family. CES outcomes are binary and shown in pp; Nationscape approval and favourability are weighted standardised scales. Specifications include geographic income and education, individual controls, religion controls, and time effects.

Table A2: JBS membership and third-party presidential voting, county fixed effects

| Year | Third party | $\beta$ |
|---|---|---|
| 1948 | Thurmond (States' Rights) | $-0.080^{*}$ |
| | | (0.037) |
| 1968 | **Wallace (American Independent)** | $-0.239^{***}$ |
| | | (0.032) |
| 1980 | **Anderson and Clark (Libertarian)** | $0.127^{***}$ |
| | | (0.007) |
| 1988 | *Base year* | — |
| | | — |
| 1992 | **Perot** | $0.067^{***}$ |
| | | (0.013) |
| 1996 | Perot | $-0.023^{***}$ |
| | | (0.007) |
| 2000 | Nader and others | $0.034^{***}$ |
| | | (0.004) |
| 2016 | Johnson, Stein and others | $0.075^{***}$ |
| | | (0.006) |

*Notes.* The standardised third-party share of the county presidential vote is regressed on JBS intensity interacted with election year, with county and year fixed effects. 58,875 county-elections across 3,101 counties and 19 elections, 1948–2020; the table reports the elections discussed in the text. County fixed effects absorb each county's own baseline propensity to vote third party. Standard errors are clustered by county and appear beneath each estimate. $^{\sim}p < 0.10$; $^{*}p < 0.05$; $^{**}p < 0.01$; $^{***}p < 0.001$.

Table A3: ANES Panel A: the pre-snapshot placebo beside the estimate

**Panel A. Spending, defence and anti-statism**

| | 1978–86 placebo | 1988–98 estimate | RW $p$ |
|---|---|---|---|
| *Means-tested spending* | | | |
| Cut food-stamp spending | 0.051 | 0.099*** | 0.005 |
| | (0.033) | (0.022) | |
| Cut spending on the poor | — | 0.096*** | 0.054 |
| | | (0.028) | |
| Cut welfare spending | — | 0.099** | 0.180 |
| | | (0.035) | |
| *Universal spending and defence* | | | |
| Cut Social Security (placebo) | 0.106** | 0.043 | 0.562 |
| | (0.034) | (0.027) | |
| Cut environment spending (placebo) | −0.015 | −0.020 | 0.894 |
| | (0.033) | (0.028) | |
| Increase defense spending | 0.007 | 0.055~ | 0.432 |
| | (0.024) | (0.029) | |
| *Anti-statism (pre-registered primary)* | | | |
| Anti-statism index (pre-reg. primary) | −0.076*** | 0.011 | 0.894 |
| | (0.023) | (0.024) | |
| Fewer government services | −0.006 | 0.053* | 0.344 |
| | (0.027) | (0.024) | |
| Jobs: each person get ahead | 0.022 | 0.076** | 0.180 |
| | (0.022) | (0.027) | |

**Panel B. Partisanship, insurgents and social attitudes**

| | 1978–86 placebo | 1988–98 estimate | RW $p$ |
|---|---|---|---|
| *Partisanship and ideology* | | | |
| Party ID (high = Republican) | −0.013 | 0.121** | 0.084 |
| | (0.029) | (0.037) | |
| Ideology (high = conservative) | 0.012 | 0.067* | 0.319 |
| | (0.019) | (0.030) | |
| *Insurgent thermometers* | | | |
| Thermometer: Ross Perot | — | 0.054 | 0.562 |
| | | (0.037) | |
| Thermometer: Pat Buchanan | — | 0.084* | 0.344 |
| | | (0.038) | |
| *Moral traditionalism, order, race* | | | |
| More emphasis on traditional values | 0.178*** | 0.089*** | 0.039 |
| | (0.035) | (0.024) | |
| Moral traditionalism index | 0.091* | 0.075** | 0.218 |
| | (0.039) | (0.029) | |
| Favors the death penalty | — | 0.037** | 0.180 |
| | | (0.013) | |
| Racial resentment (pre-reg. null) | 0.080~ | 0.024 | 0.894 |
| | (0.044) | (0.036) | |

*Notes.* ANES cumulative file, county-identified respondents, weighted by the cumulative weight normalised within wave. Outcomes are standardised; county-clustered standard errors appear beneath each estimate. The panels divide one seventeen-outcome Romano–Wolf family. The placebo applies the same specification to 1978–1986, before the 1987 membership snapshot; a dash means the item was not fielded in that period. $^{\sim}p < 0.10$; $^{*}p < 0.05$; $^{**}p < 0.01$; $^{***}p < 0.001$.

Table A4: FEC-classified receipt activity by presidential campaign

**Panel A. Dollars per capita to each campaign**

| Year | Campaign | $\beta$ | Holm $p$ | Counties |
|---|---|---|---|---|
| 1980 | Anderson (independent) | $-0.074^{***}$ | 0.003 | 3,084 |
| | | (0.020) | | |
| 1980 | Clark (Libertarian) | $-0.013$ | 1.000 | 3,084 |
| | | (0.030) | | |
| 1980 | Reagan | $0.102^{***}$ | 0.012 | 3,084 |
| | | (0.030) | | |
| 1992 | Buchanan | 0.004 | 1.000 | 3,088 |
| | | (0.018) | | |
| 1992 | Bush | 0.011 | 1.000 | 3,088 |
| | | (0.021) | | |
| 1992 | Perot | 0.008 | 1.000 | 3,088 |
| | | (0.028) | | |
| 1996 | Buchanan | 0.003 | 1.000 | 3,088 |
| | | (0.016) | | |
| 1996 | Dole | $-0.028$ | 1.000 | 3,088 |
| | | (0.024) | | |
| 1996 | Browne (Libertarian) | $-0.014$ | 1.000 | 3,088 |
| | | (0.020) | | |
| 1996 | Perot (Reform) | 0.028 | 1.000 | 3,088 |
| | | (0.037) | | |
| 2012 | Gary Johnson (Libertarian) | $-0.032^{*}$ | 0.592 | 3,088 |
| | | (0.016) | | |
| 2012 | Romney | $-0.008$ | 1.000 | 3,088 |
| | | (0.021) | | |
| 2012 | Ron Paul | $0.059^{*}$ | 0.666 | 3,088 |
| | | (0.030) | | |

**Panel B. Insurgent share of receipt dollars**

| Year | Share | $\beta$ | Holm $p$ | Counties |
|---|---|---|---|---|
| 1980 | Clark / (Clark+Reagan) | 0.001 | 1.000 | 1,211 |
| | | (0.005) | | |
| 1980 | Anderson / (Anderson+Reagan) | $-0.063^{***}$ | <0.001 | 1,310 |
| | | (0.014) | | |
| 1992 | Buchanan / (Buchanan+Bush) | 0.010 | 1.000 | 1,772 |
| | | (0.012) | | |
| 1992 | Perot / (Perot+Bush) | 0.003 | 1.000 | 1,721 |
| | | (0.012) | | |
| 1996 | Buchanan / (Buchanan+Dole) | $0.028^{*}$ | 0.469 | 1,980 |
| | | (0.013) | | |
| 2012 | Ron Paul / (Paul+Romney) | 0.001 | 1.000 | 3,026 |
| | | (0.005) | | |

*Notes.* The source is the FEC's itemized-individual receipt transaction family; receipt records are neither unique donors nor exclusively natural persons. Campaigns are identified using official candidate and committee identifiers and presidential-committee status. Libertarian rows refer to Edward Clark, Harry Browne and Gary Johnson. Panel A outcomes are $\log(1 + \max\{\$\,\text{per capita}, 0\})$, standardised; signed records are aggregated before the county-campaign net-dollar floor is applied. Panel B is the insurgent share of combined insurgent and mainstream receipt dollars among counties giving to either campaign. Holm $p$ controls familywise error over the joint 19-test menu of all campaign levels and shares. All specifications include ARDA county religion, contemporaneous log population, South, cycle-specific log per-capita income and bachelor's share; standard errors are clustered by county. $^{\sim}p < 0.10$; $^{*}p < 0.05$; $^{**}p < 0.01$; $^{***}p < 0.001$.

**Exploratory Analysis of Public Medicare Part D Ivermectin Claims**

A contemporary review links Bircher opposition to fluoridation and promotion of laetrile as a cancer treatment to present-day ivermectin enthusiasm (Green 2023). This journalistic analogy motivates a descriptive comparison, not a claim that the same people, organizations, or mechanisms connect the episodes. The 1987 rolls and provider-located CMS claims identify neither current JBS ties nor beneficiary beliefs, residence, prescribing indication, or the route of generic records. Given prior evidence of county political differences in ivermectin prescribing (Barnett et al. 2022), I ask only whether the association between historical JBS intensity and publicly visible claims differed in 2021 from 2019.

I construct a 2013–2024 county-year panel from the Medicare Part D Prescribers by Provider and Drug files (Centers for Medicare & Medicaid Services 2026; Centers for Medicare & Medicaid Services, Office of Enterprise Data and Analytics 2024). CMS omits provider–drug cells with ten or fewer claims. The Provider Public Use File (PUF), which supplies the denominator, also omits prescribers with ten or fewer total Part D claims. CMS reports the prescribing provider's five-digit postal ZIP code. Postal ZIP codes are not county polygons, so I use the corresponding 2020 Census ZIP Code Tabulation Area (ZCTA) when an exact five-digit match exists and assign that ZCTA to the county containing the largest share of its land area. Rows with no exact ZCTA match do not enter the county totals. I apply this same assignment to the ivermectin numerator and the Provider-PUF denominator before merging the county JBS totals.

The outcome therefore counts published claims in the prescribing provider's county, not the beneficiary's county, and it does not measure all ivermectin use there. A county-year zero means that no mapped provider–drug cell was published; it does not establish that no ivermectin was prescribed. The public file also does not report dosage form. In 2021, 99.18% of published claims assigned using this common geography appear under the generic label "Ivermectin." I treat those records as generic and route ambiguous. I compare them with Soolantra and Sklice, whose official labels identify them as topical products (U.S. National Library of Medicine 2024b; U.S. National Library of Medicine 2024a). This distinction cannot establish that the generic records were oral or identify why any product was prescribed.

The event model takes $\log(1 + \text{JBS membership records})$ and standardizes it once across the counties in the analysis. It estimates a separate association for each year from 2013 through 2024, omits 2019, and includes county and state-by-year fixed effects. The baseline specification also interacts logged 2019 Part D claims and prescriber counts with year. Standard errors are clustered by state. Except for the publication indicator, each outcome is the inverse-hyperbolic-sine transformation of published claims per 100,000 Provider-PUF Part D claims; the transformation is log-like but retains zeros. The publication indicator is estimated as a linear probability. Each event coefficient is the difference between that year's county JBS association and the 2019 association, not a treatment effect. Appendix Figure A4 displays the generic, definite-topical, and generic-minus-topical event paths; Appendix Table A5 reports the robustness stack.

The national result is null. In the baseline model, the 2021-versus-2019 broad coefficient across 3,063 counties is 0.028 (SE = 0.051). The difference between the generic/route-ambiguous and definite-topical coefficients is 0.030 (SE = 0.052; wild-bootstrap $p = 0.570$). The enriched specification replaces the two linear volume controls with provider-volume splines and adds the logged 2019 Herfindahl–Hirschman index for the concentration of Part D claims across providers, 2019 generalist and dermatology provider shares, logged 2015 population, and the 2015 age-65 share, all interacted with year. Across the 3,053 counties with complete enriched controls, the broad coefficient remains imprecise at 0.068 (SE = 0.050; wild-bootstrap $p = 0.176$), as does the generic-minus-topical coefficient of 0.058 (SE = 0.051; wild-bootstrap $p = 0.239$).

The publication process is much less likely to reveal an ivermectin cell in counties with smaller Part D markets. In 2021, 5.6% of counties in the smallest decile of 2019 Part D claim volume have any visible ivermectin cell, compared with 92.2% in the largest decile. I therefore report the full sequence of provider-volume restrictions and do not treat the median split as a preferred specification. Among the 1,532 counties at or above the 2019 Part D-claims median of 115,728, the baseline broad coefficient is 0.161 (SE = 0.064), and the generic-minus-topical coefficient is 0.159 (SE = 0.069; wild-bootstrap $p = 0.024$). With the enriched controls, 1,531 counties remain: the broad coefficient is 0.146 (SE = 0.069; wild-bootstrap $p = 0.047$), and the generic-minus-topical coefficient is 0.144 (SE = 0.073; wild-bootstrap $p = 0.058$). The definite-topical component is near zero in both models. In the enriched linear-probability model, the corresponding change in the JBS association with whether CMS published any ivermectin cell is 0.051 (SE = 0.024; wild-bootstrap $p = 0.045$). This publication indicator is partly mechanical because a county changes from zero to one when any provider–drug cell clears the disclosure threshold.

Weighting and transformation checks weaken the larger-market pattern. In the enriched top-half model weighted by fixed 2019 Part D claim volume, the broad coefficient is 0.080 (SE = 0.084), and the generic-minus-topical coefficient is 0.050 (SE = 0.099). Using the untransformed broad claim rate in the unweighted enriched top-half model gives 0.752 (SE = 0.729). Thus, the positive larger-market estimates are features of some unweighted transformed-outcome specifications, not independent confirmations.

The pre-event paths also limit the topical comparison. Joint state-clustered Wald tests of the 2013–2018 coefficients relative to 2019 give $p = 0.185$ for the all-county broad outcome and $p = 0.770$ for the top-half broad outcome. For generic/route-ambiguous claims, the corresponding values are $p = 0.573$ and $p = 0.820$; the top-half covariance has effective rank five. The definite-topical component rejects joint equality in the all-county baseline model ($p = 0.010$) but not in the top-half model ($p = 0.216$); the generic-minus-topical contrast does not reject in either sample ($p = 0.441$ and $p = 0.362$). I therefore use the definite-topical outcome as a comparison, not as a clean placebo.

The wild-bootstrap values above use 9,999 null-imposed draws with Rademacher weights at the state level; they are reported only where run and are not multiplicity adjusted. Separately, Benjamini–Hochberg adjustment covers 30 baseline-control tests: six provider-volume restrictions for each of five outcomes. The smallest adjusted value is $q = 0.094$. This family excludes the enriched, weighting, raw-outcome, and other exploratory specifications, so the broader search is larger.

The CMS files therefore show no detectable nationwide 2021-versus-2019 change. Positive generic–topical contrasts appear only in some unweighted larger-market models and change across specifications. Because observation depends on CMS's disclosure threshold and claims are provider-located, they do not establish organizational continuity, a causal pandemic response, or resident ivermectin use.

Table A5: JBS membership intensity and publicly visible ivermectin claims: robustness checks

| Specification and outcome | $\beta$ | (SE) | Wild-bootstrap $p$ | BH $q$ | Counties |
|---|---|---|---|---|---|
| **Panel A. Provider-volume, composition, and capacity controls** | | | | | |
| *All counties: baseline linear volume controls* | | | | | |
| Broad visible claim rate | 0.028 | (0.051) | — | — | 3,063 |
| Generic / route-ambiguous claim rate | 0.027 | (0.051) | 0.590 | — | 3,063 |
| Definite-topical claim rate | −0.002 | (0.006) | 0.735 | — | 3,063 |
| Generic minus definite topical | 0.030 | (0.052) | 0.570 | — | 3,063 |
| Any published provider–drug cell | 0.006 | (0.016) | — | — | 3,063 |
| *Top half of 2019 Part D claims: baseline linear volume controls* | | | | | |
| Broad visible claim rate | 0.161* | (0.064) | — | — | 1,532 |
| Generic / route-ambiguous claim rate | 0.157* | (0.067) | 0.023 | — | 1,532 |
| Definite-topical claim rate | −0.003 | (0.012) | 0.823 | — | 1,532 |
| Generic minus definite topical | 0.159* | (0.069) | 0.024 | — | 1,532 |
| Any published provider–drug cell | 0.049* | (0.023) | — | — | 1,532 |
| *All counties: enriched provider-volume controls* | | | | | |
| Broad visible claim rate | 0.068 | (0.050) | 0.176 | — | 3,053 |
| Generic / route-ambiguous claim rate | 0.062 | (0.050) | 0.212 | — | 3,053 |
| Definite-topical claim rate | 0.004 | (0.007) | 0.545 | — | 3,053 |
| Generic minus definite topical | 0.058 | (0.051) | 0.239 | — | 3,053 |
| Any published provider–drug cell | 0.025~ | (0.015) | 0.096 | — | 3,053 |
| *Top half of 2019 Part D claims: enriched provider-volume controls* | | | | | |
| Broad visible claim rate | 0.146* | (0.069) | 0.047 | — | 1,531 |
| Generic / route-ambiguous claim rate | 0.143* | (0.071) | 0.057 | — | 1,531 |
| Definite-topical claim rate | −0.001 | (0.012) | 0.911 | — | 1,531 |
| Generic minus definite topical | 0.144* | (0.073) | 0.058 | — | 1,531 |
| Any published provider–drug cell | 0.051* | (0.024) | 0.045 | — | 1,531 |
| *Top half: enriched controls, fixed 2019-claim weights* | | | | | |
| Broad visible claim rate | 0.080 | (0.084) | — | — | 1,531 |
| Generic / route-ambiguous claim rate | 0.058 | (0.094) | — | — | 1,531 |
| Definite-topical claim rate | 0.009 | (0.020) | — | — | 1,531 |
| Generic minus definite topical | 0.050 | (0.099) | — | — | 1,531 |
| Any published provider–drug cell | 0.046~ | (0.028) | — | — | 1,531 |

*Continued on next page*

*Appendix table continued*

| Specification and outcome | $\beta$ | (SE) | Wild-bootstrap $p$ | BH $q$ | Counties |
|---|---|---|---|---|---|
| **Panel B. Baseline 2019 provider-volume thresholds** | | | | | |
| *All counties ($N = 3,063$)* | | | | | |
| Broad visible claim rate | 0.028 | (0.051) | — | 0.773 | 3,063 |
| Generic / route-ambiguous claim rate | 0.027 | (0.051) | — | 0.773 | 3,063 |
| Definite-topical claim rate | −0.002 | (0.006) | — | 0.820 | 3,063 |
| Any published provider–drug cell | 0.006 | (0.016) | — | 0.820 | 3,063 |
| *Top 75% by 2019 Part D claims ($N = 2,297$)* | | | | | |
| Broad visible claim rate | 0.078 | (0.056) | — | 0.286 | 2,297 |
| Generic / route-ambiguous claim rate | 0.075 | (0.057) | — | 0.302 | 2,297 |
| Definite-topical claim rate | −0.001 | (0.008) | — | 0.969 | 2,297 |
| Any published provider–drug cell | 0.020 | (0.019) | — | 0.420 | 2,297 |
| *Top 50% by 2019 Part D claims ($N = 1,532$)* | | | | | |
| Broad visible claim rate | 0.161* | (0.064) | — | 0.094 | 1,532 |
| Generic / route-ambiguous claim rate | 0.157* | (0.067) | — | 0.094 | 1,532 |
| Definite-topical claim rate | −0.003 | (0.012) | — | 0.887 | 1,532 |
| Any published provider–drug cell | 0.049* | (0.023) | — | 0.094 | 1,532 |
| *Top 25% by 2019 Part D claims ($N = 766$)* | | | | | |
| Broad visible claim rate | 0.175* | (0.087) | — | 0.094 | 766 |
| Generic / route-ambiguous claim rate | $0.169^{\sim}$ | (0.090) | — | 0.114 | 766 |
| Definite-topical claim rate | 0.008 | (0.022) | — | 0.820 | 766 |
| Any published provider–drug cell | 0.072* | (0.032) | — | 0.094 | 766 |
| *At least 50 Part D prescribers in 2019 ($N = 1,540$)* | | | | | |
| Broad visible claim rate | 0.133* | (0.059) | — | 0.094 | 1,540 |
| Generic / route-ambiguous claim rate | 0.125* | (0.061) | — | 0.094 | 1,540 |
| Definite-topical claim rate | 0.005 | (0.011) | — | 0.820 | 1,540 |
| Any published provider–drug cell | 0.042* | (0.021) | — | 0.094 | 1,540 |
| *At least 100 Part D prescribers in 2019 ($N = 1,095$)* | | | | | |
| Broad visible claim rate | 0.186* | (0.086) | — | 0.094 | 1,095 |
| Generic / route-ambiguous claim rate | 0.182* | (0.089) | — | 0.094 | 1,095 |
| Definite-topical claim rate | 0.000 | (0.017) | — | 0.984 | 1,095 |
| Any published provider–drug cell | 0.064* | (0.030) | — | 0.094 | 1,095 |

*Continued on next page*

*Appendix table continued*

| Specification and outcome | $\beta$ | (SE) | Wild-bootstrap $p$ | BH $q$ | Counties |
|---|---|---|---|---|---|
| **Panel C. Historical-population exposure definitions** | | | | | |
| *JBS members per 100,000 residents (1980)* | | | | | |
| Broad visible claim rate | 0.013 | (0.020) | — | — | 3,032 |
| Any published provider–drug cell | 0.003 | (0.005) | — | — | 3,032 |
| log(1 + *JBS members per 100,000 residents*) | | | | | |
| Broad visible claim rate | 0.043 | (0.030) | — | — | 3,032 |
| Any published provider–drug cell | $0.016^{\sim}$ | (0.009) | — | — | 3,032 |

*Notes.* Each coefficient is the difference between the 2021 and 2019 associations of county JBS membership with the outcome. Except for the publication indicator, outcomes are asinh of aligned, publicly visible ivermectin claims per 100,000 Provider-PUF Part D claims. The indicator is on the probability scale; Panel B converts its saved asinh coefficient and standard error back by dividing by asinh(1). All models include county-unit and state-by-year fixed effects and state-clustered standard errors. Panel A's enriched model interacts provider-volume splines, provider-claim HHI, generalist and dermatology shares, population, and the age-65 share with year. The $\beta$ column reports that association difference, and (SE) reports its state-clustered standard error. Wild-bootstrap $p$ reports 9,999-draw null-imposed Rademacher wild state-cluster inference where it was run: the baseline generic, topical, and difference rows and all enriched unweighted rows in Panel A. BH $q$ reports Benjamini–Hochberg adjustment across Panel B's full 30-test family—six provider-volume restrictions for each of five outcomes, including the unshown inclusive oral-upper outcome. Numerical conventional $p$-values are not shown. Stars refer to the conventional state-clustered test: $^{\sim}p < 0.10$; $^{*}p < 0.05$; $^{**}p < 0.01$; $^{***}p < 0.001$. A dash means the indicated wild-bootstrap or BH inference was not run or is not applicable. Panel B uses linear 2019 Part D claims and prescribers by year. Panel C harmonizes JBS membership and 1980 population to ARDA longitudinal county units before aggregation. The provider rebuild mapped 1,207,475 rows (98.3%; 99.3% claim weighted) and exactly reproduced claims and prescriber totals in 3,063 counties. The enriched top-half contrast is positive in every leave-one-state-out estimate (0.124 to 0.176). The historical check retains 45,042 of 45,137 source members. Generic records remain route ambiguous. Published CMS provider–drug cells with ten or fewer claims are omitted. Claims are assigned to the provider's county, not the beneficiary's county.

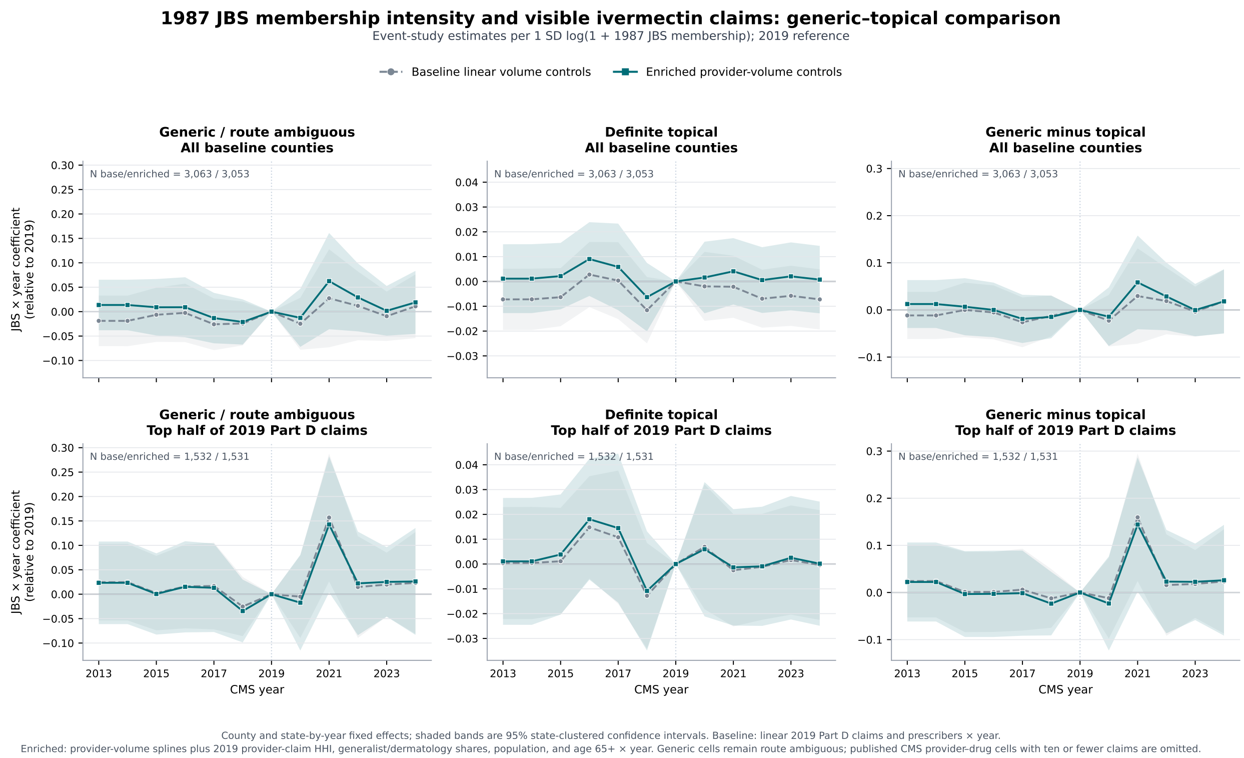


Figure A4: 1987 JBS membership intensity and visible ivermectin claims: generic–topical comparison

*Notes.* Coefficients are interactions between standardized $\log(1 + 1987 \text{ JBS members})$ and CMS year; 2019 is omitted. The outcomes are asinh of aligned, published claims per 100,000 Provider-PUF Part D claims for generic/route-ambiguous ivermectin, definite-topical ivermectin, and the difference between those two transformed outcomes. All models include county and state-by-year fixed effects; shaded bands are 95% confidence intervals from state-clustered standard errors. The baseline specification interacts linear 2019 Part D claim and prescriber volume with year. The enriched specification replaces those terms with provider-volume splines and adds 2019 provider-claim HHI, generalist and dermatology provider shares, population, and the age-65 share, all interacted with year. The lower row retains counties at or above the 2019 Part D-claims median of 115,728. Published CMS provider–drug cells with ten or fewer claims are omitted. Claims are assigned to the provider's county, not the beneficiary's county, and generic records do not identify route.

Table A6: Replication benchmark using the published linear-population form

| | Model 1 Pape et al. replication | Model 2 + JBS (log, z) | Model 3 JBS only + controls | Model 4 Certification interaction |
|---|---|---|---|---|
| *Main Explanatory Variables* | | | | |
| White Population Decline 2010–2020 | $1.368^{***}$ | $1.332^{***}$ | | $1.338^{***}$ |
| | (0.074) | (0.072) | | (0.073) |
| Manufacturing Employment Decline, 1970–2020 | $1.122^{*}$ | 1.064 | | 1.067 |
| | (0.063) | (0.065) | | (0.066) |
| Trump 2020–Romney 2012 Vote-Share Gap | $0.768^{***}$ | $0.829^{***}$ | | $0.834^{***}$ |
| | (0.042) | (0.045) | | (0.046) |
| JBS Membership (log, z) | | $1.504^{***}$ | $1.646^{***}$ | $1.443^{***}$ |
| | | (0.104) | (0.116) | (0.141) |
| House Rep Objected | | | | 1.007 |
| | | | | (0.129) |
| JBS × Objected | | | | 1.110 |
| | | | | (0.108) |
| *Controls* | | | | |
| % Non-Hispanic White | $1.215^{**}$ | $1.161^{*}$ | 1.048 | $1.165^{*}$ |
| | (0.078) | (0.076) | (0.064) | (0.076) |
| Urban County | $2.882^{***}$ | $2.639^{***}$ | $3.423^{***}$ | $2.684^{***}$ |
| | (0.384) | (0.351) | (0.432) | (0.357) |
| Distance to DC | $0.739^{***}$ | $0.692^{***}$ | $0.697^{***}$ | $0.690^{***}$ |
| | (0.046) | (0.043) | (0.041) | (0.044) |
| County Population | $1.693^{***}$ | $1.411^{***}$ | $1.420^{***}$ | $1.405^{***}$ |
| | (0.122) | (0.095) | (0.108) | (0.098) |
| *N* | 3,112 | 3,112 | 3,112 | 3,069 |
| AIC | 3,128.7 | 3,083.2 | 3,131.7 | 3,042.3 |
| Log-Likelihood | −1,556.4 | −1,532.6 | −1,559.9 | −1,510.1 |

*Notes:* Coefficients are incidence rate ratios (IRR) from negative binomial regressions, with HC1 robust standard errors on the IRR scale in parentheses. All columns retain Pape, Larson, and Ruby (2024)'s linear control for county population; Table A12 reports the corresponding free-log and exposure models. Continuous covariates and logged JBS are standardized before complete-case restriction. Models including the certification vote use the 3,069 counties with non-missing House-vote data. Following Pape, Larson, and Ruby (2024), estimation excludes Alaska. $^{\sim}p < 0.10$; $^{*}p < 0.05$; $^{**}p < 0.01$; $^{***}p < 0.001$.

Table A7: Published and replicated January 6 coefficients

| Variable | Published Model 4 | Replication Model 1 |
|---|---|---|
| White population decline | $1.37^{***}$ | $1.368^{***}$ |
| | | (0.074) |
| Manufacturing employment decline | $1.12^{*}$ | $1.122^{*}$ |
| | | (0.063) |
| Trump 2020–Romney 2012 vote-share gap | $0.77^{***}$ | $0.768^{***}$ |
| | | (0.042) |
| % non-Hispanic white | $1.21^{**}$ | $1.215^{**}$ |
| | | (0.078) |
| Urban county | $2.88^{***}$ | $2.882^{***}$ |
| | | (0.384) |
| Distance to Washington, DC | $0.74^{***}$ | $0.739^{***}$ |
| | | (0.046) |
| County population | $1.69^{***}$ | $1.693^{***}$ |
| | | (0.122) |
| *N* | 3,112 | 3,112 |

*Notes:* Entries are incidence rate ratios. Published values are from Pape et al. (2024, Table 2, Model 4). Replication values are Model 1 from Table A6, with HC1 robust standard errors shown in parentheses. Stars in the published column are reproduced from the source; $^{\sim}p < 0.10$; $^{*}p < 0.05$; $^{**}p < 0.01$; $^{***}p < 0.001$.

Table A8: Pape outbidding interaction and JBS membership

| | Published Model 9 | M5a replication | M5b + JBS |
|---|---|---|---|
| White population decline | $1.28^{***}$ | $1.350^{***}$ | $1.287^{**}$ |
| House Republican objected | 0.92 | 0.948 | 1.012 |
| White decline × objected | $1.25^{*}$ | $1.192^{\sim}$ | $1.184^{\sim}$ |
| JBS membership (log, z) | — | — | $1.604^{***}$ |
| *N* | 3,071 | 3,069 | 3,069 |

*Notes:* Entries are incidence rate ratios under the published linear-population form. Published values are from Pape et al. (2024, Table 3, Model 9). M5a reproduces the outbidding interaction on the non-missing House-vote sample; M5b adds standardized logged JBS membership. $^{\sim}p < 0.10$; $^{*}p < 0.05$; $^{**}p < 0.01$; $^{***}p < 0.001$.

Table A9: Coefficient movement in the replicated January 6 linear-population model

| Variable | Without JBS (Model 1) | With JBS (Model 2) |
|---|---|---|
| White Population Decline | 1.368 | 1.332 |
| | [<0.001] | [$1.3 \times 10^{-7}$] |
| Manufacturing Decline | 1.122 | 1.064 |
| | [0.040] | [0.308] |
| Trump 2020–Romney 2012 vote-share gap | 0.768 | 0.829 |
| | [<0.001] | [<0.001] |
| **JBS Membership** | — | **1.504** |
| | | **[<0.001]** |
| AIC | 3,128.7 | 3,083.2 |
| $\Delta$AIC | — | −45.6 |

*Notes:* Entries are incidence rate ratios from the replicated January 6 negative binomial specification, which enters county population linearly in units of 100,000. Square-bracketed values beneath the IRRs are two-sided $p$-values calculated from HC1 robust standard errors. Both models include controls for % non-Hispanic white, urban status, and distance to Washington, DC.

Table A10: Republican two-party vote-share change and JBS membership: weighted specifications and estimand sensitivity

*Panel A. Population-weighted specifications*

| | (1) Replication | (2) + JBS (log, z) | (3) + Any JBS | (4) + JBS p.c. | (5) + 2012 baseline |
|---|---|---|---|---|---|
| JBS membership (log, z) | | $-0.912^{***}$ | | | $-0.759^{***}$ |
| | | (0.162) | | | (0.135) |
| Any JBS (1=yes) | | | $0.494^{\sim}$ | | |
| | | | (0.295) | | |
| JBS per 10,000 (log, z) | | | | $-0.786^{***}$ | |
| | | | | (0.146) | |
| Romney 2012 share | | | | | $-0.148^{***}$ |
| | | | | | (0.008) |
| Mfg. decline 1970–2015 | $0.045^{**}$ | $0.040^{**}$ | $0.045^{**}$ | $0.040^{**}$ | 0.019 |
| | (0.015) | (0.014) | (0.015) | (0.014) | (0.012) |
| Log population (2015) | $-0.284^{\sim}$ | $0.355^{\sim}$ | $-0.303^{\sim}$ | $-0.297^{*}$ | 0.004 |
| | (0.159) | (0.187) | (0.161) | (0.148) | (0.168) |
| Additional demographic controls | Yes | Yes | Yes | Yes | Yes |
| *N* | 2,608 | 2,608 | 2,608 | 2,608 | 2,608 |

*Notes:* The dependent variable is Trump's 2016 two-party vote share minus Romney's 2012 share. Population-weighted OLS with HC1 robust standard errors in parentheses follows Broz, Frieden, and Weymouth (2021). Every specification includes age 65+, white and Hispanic population shares, log wage, female and college shares, business/services employment share, manufacturing decline, and log 2015 population; column (5) also includes Romney's 2012 two-party share. The per-capita exposure scales 1987 JBS membership by 2015 population.
$^{\sim}p < 0.10$; $^{*}p < 0.05$; $^{**}p < 0.01$; $^{***}p < 0.001$.

**Table A10 (continued):** Republican two-party vote-share change and JBS membership: weighted specifications and estimand sensitivity

| *Panel B. Weighting estimand and population-concentration sensitivity* | | | | |
|---|---|---|---|---|
| Estimand and sample | JBS exposure | $\beta$ | $N$ | Original weight removed |
| Average resident; full sample | Log count (z) | $-0.912^{***}$ (0.162) | 2,608 | 0.0% |
| Average county; full sample | Log count (z) | $-0.089$ (0.087) | 2,608 | — |
| Average county; full sample | Log p.c. (z) | $-0.033$ (0.070) | 2,608 | — |
| Average resident; drop top 5% | Log count (z) | $-0.213^{\sim}$ (0.120) | 2,477 | 49.2% |
| Average resident; drop top 10% | Log count (z) | $-0.156$ (0.121) | 2,347 | 63.4% |

*Notes:* The dependent variable is Trump's 2016 two-party vote share minus Romney's 2012 share. Panel B retains Panel A, column (2)'s controls and full-sample exposure standardization. Coefficients are percentage-point changes per standard deviation of the indicated logged JBS measure; HC1 robust standard errors appear in parentheses immediately beneath. Symbols use conventional two-sided tests calculated from those HC1 standard errors: $^{\sim}p < 0.10$; $^{*}p < 0.05$; $^{**}p < 0.01$; $^{***}p < 0.001$.

The average-county rows omit population weights. The fixed top-5% and top-10% rows exclude exactly 131 and 261 counties above the full-sample 95th and 90th percentiles of the 2000 population weight; they do not restandardize JBS exposure. Those counties hold 49.2% and 63.4% of the original weights. Dropping California ($\beta = -0.778$) or Los Angeles County ($\beta = -0.938$) leaves the full-sample weighted estimate negative.

Table A11: Right-wing terrorism logits and JBS membership (Nemeth & Hansen 2021 replication)

| Specification | Coefficient | Two-sided $p$ | $N$ |
|---|---|---|---|
| Main model: JBS membership (log, z) | $-0.016$<br>(0.141) | [0.911] | 133,539 |
| Any JBS indicator | $-0.174$<br>(0.411) | [0.672] | 133,539 |
| JBS × electoral competition | $-0.229$<br>(0.287) | [0.424] | 133,539 |
| JBS × racial composition | $-0.006$<br>(0.005) | [0.255] | 133,539 |
| 1988–2016 window: JBS membership | $-0.211$<br>(0.179) | [0.240] | 85,457 |
| 1971–1987 window: JBS membership | 0.238<br>(0.251) | [0.343] | 48,082 |

*Notes:* Entries are logit coefficients, with county-clustered standard errors in parentheses beneath and two-sided $p$-values in square brackets. All specifications include the Nemeth & Hansen control vector: lagged political competition, racial composition, county GDP per capita, labor-force participation, citizenship, population, urbanization, land area, spatial lag of right-wing violence, election-year indicators, presidential-party controls, region indicators, and cubic time trends.

Table A12: January 6 defendant-count models across population treatments

| Specification | White decline | Manufacturing decline | Trump 2020–Romney 2012 vote-share gap | JBS term | Linear-pop. IRR | Elasticity $\delta$ | AIC |
|---|---|---|---|---|---|---|---|
| *Panel A. Substantive covariates, population terms, and model fit* | | | | | | | |
| | 1.368 | 1.122 | 0.768 | | 1.693 | | |
| **M1**: linear; no JBS | [<0.001] | [0.040] | [<0.001] | — | [<0.001] | — | 3128.7 |
| | 1.332 | 1.064 | 0.829 | 1.504 | 1.411 | | |
| **M2**: linear + log JBS | [<0.001] | [0.308] | [<0.001] | [<0.001] | [<0.001] | — | 3083.2 |
| | 1.110 | 0.935 | 1.033 | | | 1.005 | |
| **P-L1**: free log; no JBS | [0.048] | [0.286] | [0.532] | — | — | [0.933] | 2900.4 |
| | 1.103 | 0.938 | 1.031 | 0.930 | | 1.053 | |
| **P-L2**: free log + JBS | [0.063] | [0.312] | [0.550] | [0.284] | — | [0.456] | 2901.1 |
| | 1.110 | 0.936 | 1.032 | | | 1.000 | |
| **P-O1**: offset; no JBS | [0.048] | [0.267] | [0.532] | — | — | [fixed] | 2898.4 |
| | 1.109 | 0.944 | 1.024 | 0.962 | | 1.000 | |
| **P-O2**: offset + log JBS | [0.046] | [0.351] | [0.641] | [0.454] | — | [fixed] | 2899.8 |
| | 1.109 | 0.937 | 1.032 | 0.948 | | 1.000 | |
| **P-O3**: offset + per-capita JBS | [0.052] | [0.270] | [0.531] | [0.543] | — | [fixed] | 2899.9 |
| | 1.112 | 0.942 | 1.026 | 0.815 | | 1.000 | |
| **P-O4**: offset + any JBS | [0.041] | [0.319] | [0.613] | [0.213] | — | [fixed] | 2898.8 |

*Notes:* Cells report incidence-rate ratios with HC1 robust $p$-values in square brackets beneath. The linear-population IRR is reported only for M1–M2. P-L1–P-L2 estimate the coefficient on raw log(2020 population), while P-O1–P-O4 fix that elasticity at one through an exposure offset. Complete model definitions accompany Panel B.

**Table A12 (continued):** January 6 defendant-count models across population treatments

| Specification | % non-Hispanic white | Urban county | Distance to DC |
|---|---|---|---|
| *Panel B. Remaining covariates (IRRs; robust p-values beneath)* | | | |
| **M1**: linear; no JBS | 1.215<br>[0.003] | 2.882<br>[<0.001] | 0.739<br>[<0.001] |
| **M2**: linear + log JBS | 1.161<br>[0.022] | 2.639<br>[<0.001] | 0.692<br>[<0.001] |
| **P-L1**: free log; no JBS | 1.315<br>[<0.001] | 1.380<br>[0.017] | 0.816<br>[<0.001] |
| **P-L2**: free log + JBS | 1.327<br>[<0.001] | 1.362<br>[0.022] | 0.829<br>[<0.001] |
| **P-O1**: offset; no JBS | 1.311<br>[<0.001] | 1.387<br>[0.007] | 0.817<br>[<0.001] |
| **P-O2**: offset + log JBS | 1.300<br>[<0.001] | 1.416<br>[0.005] | 0.826<br>[<0.001] |
| **P-O3**: offset + per-capita JBS | 1.318<br>[<0.001] | 1.375<br>[0.009] | 0.824<br>[<0.001] |
| **P-O4**: offset + any JBS | 1.312<br>[<0.001] | 1.399<br>[0.006] | 0.821<br>[<0.001] |

*Notes:* All models are negative-binomial regressions of January 6 defendant counts using the same 3,112 counties. The Trump–Romney covariate is Trump's 2020 vote share minus Romney's 2012 vote share. Cells report incidence-rate ratios with HC1 robust $p$-values in square brackets beneath; the elasticity column instead reports the two-sided $p$-value for $H_0 : \delta = 1$. Continuous substantive covariates and logged JBS measures are standardized before complete-case restriction. M1–M2 use the published linear population control; P-L1–P-L2 estimate the coefficient on log(2020 population); P-O1–P-O4 use it as an exposure offset. P-O3 scales 1987 JBS membership per 10,000 2020 residents.

Table A13: JBS membership across party and certification-vote groups on matched district geography

| *Panel A. Republican versus Democratic districts ($N = 420$)* | | | |
|---|---|---|---|
| Measure | Republican mean | Democratic mean | Ratio/IRR |
| JBS members | 134.7 | 76.7 | 1.756 [<0.001] |
| JBS members per 100,000 | 17.92 | 10.32 | 1.737 [<0.001] |
| Population-offset NB2 | – | – | 1.737 [<0.001] |
| Male members per 100,000 | 10.56 | 5.93 | 1.781 [<0.001] |
| Female members per 100,000 | 6.36 | 3.87 | 1.643 [<0.001] |
| Local-chapter members per 100,000 | 11.32 | 5.82 | 1.944 [<0.001] |
| HOME-chapter members per 100,000 | 6.28 | 4.30 | 1.461 [<0.001] |
| *Panel B. Republican certification vote (132 objectors; 71 certifiers)* | | | |
| Measure | Objector mean | Certifier mean | Ratio/IRR |
| JBS members | 127.6 | 147.8 | 0.864 [0.121] |
| JBS members per 100,000 | 16.99 | 19.65 | 0.864 [0.110] |
| Population-offset NB2 | – | – | 0.864 [0.241] |
| Male members per 100,000 | 9.98 | 11.65 | 0.857 [0.147] |
| Female members per 100,000 | 6.04 | 6.97 | 0.867 [0.087] |
| Local-chapter members per 100,000 | 10.83 | 12.23 | 0.886 [0.145] |
| HOME-chapter members per 100,000 | 5.86 | 7.06 | 0.830 [0.230] |

*Notes:* North Carolina is excluded because its boundaries changed between the 116th and 117th Congresses. JBS ZIP aggregates are allocated fractionally across intersecting districts using the Census Bureau's national 116th-Congress ZCTA relationship file; population is the 2018 ACS one-year B01003 estimate. Ordinary rows report two-sided Mann–Whitney $U$ tests. NB2 rows use log population as an offset and HC0 robust standard errors; entries are incidence-rate ratios for the first group relative to the second group in each panel. Two-sided $p$-values appear beneath the ratios and IRRs.

# References


Acharya, Avidit, Matthew Blackwell, and Maya Sen (July 2016). “The Political Legacy of American Slavery”. *The Journal of Politics* 78.3, pp. 621–641. DOI: 10.1086/686631.

Algara, Carlos and Sharif Amlani (2021). *Replication Data for: Partisanship and Nationalization in American Elections: Evidence from Presidential, Senatorial and Gubernatorial Elections in the U.S. Counties, 1872–2020*. Dataset. County presidential returns, 1868–2020; the third-party share is derived as total minus Democratic minus Republican. DOI: 10.7910/DVN/DGUMFI. URL: https://doi.org/10.7910/DVN/DGUMFI.

American National Election Studies (2022). *ANES Time Series Cumulative Data File (1948–2020)*. Dataset. DOI: 10.3886/ICPSR08475. URL: https://electionstudies.org.

Ansolabehere, Stephen, Brian F. Schaffner, and Sam Luks (2021). *Cooperative Election Study, Common Content*. Dataset; policy-preferences companion file from the same record. URL: https://cces.gov.harvard.edu.

Bacon, Rachel J., Roger Finke, and Dale E. Jones (2018). “Merging the Religious Congregations and Membership Studies: A Data File for Documenting American Religious Change”. *Review of Religious Research* 60.3, pp. 403–423. DOI: 10.1007/s13644-018-0339-4.

Barnett, Michael L. et al. (2022). “Association of County-Level Prescriptions for Hydroxychloroquine and Ivermectin With County-Level Political Voting Patterns in the 2020 US Presidential Election”. *JAMA Internal Medicine* 182.4, pp. 452–454. DOI: 10.1001/jamainternmed.2022.0200. URL: https://doi.org/10.1001/jamainternmed.2022.0200.

Broz, J. Lawrence, Jeffry Frieden, and Stephen Weymouth (Apr. 2021). “Populism in Place: The Economic Geography of the Globalization Backlash”. *International Organization* 75.2, pp. 464–494. DOI: 10.1017/S0020818320000314.

Centers for Medicare & Medicaid Services (2026). *Medicare Part D Prescribers—by Provider and Drug*. Dataset. Annual public-use files for data years 2013–2024; the landing page was last modified May 21, 2026. Baltimore, MD. URL: https://data.cms.gov/provider-summary-by-type-of-service/medicare-part-d-prescribers/medicare-part-d-prescribers-by-provider-and-drug (visited on 08/09/2026).

Centers for Medicare & Medicaid Services, Office of Enterprise Data and Analytics (May 2024). *Medicare Part D Prescribers Datasets: A Methodological Overview*. Methodological Overview. Baltimore, MD: Centers for Medicare & Medicaid Services. URL: https://data.cms.gov/sites/default/files/2024-06/MUP_DPR_RY24_20240510_Methodology_508.pdf (visited on 08/09/2026).

Dallek, Matthew (2023). *Birchers: How the John Birch Society radicalized the American right*. Basic Books.

Dell, Melissa (Mar. 2025). “Deep Learning for Economists”. *Journal of Economic Literature* 63.1, pp. 5–58. DOI: 10.1257/jel.20241733.

Dell, Melissa et al. (2023). “American Stories: A Large-Scale Structured Text Dataset of Historical U.S. Newspapers”. *Advances in Neural Information Processing Systems*.

DePue, Mark (2011). *Interview with Phyllis Schlafly*. Abraham Lincoln Presidential Library Oral History Program, ISE-A-L-2011-001.01.

Federal Election Commission (2026). *Bulk Data: Contributions by Individuals and Committee Master, Cycles 1980–2012*. Dataset. Continuously updated series; the year given is the year of retrieval. Files used: indiv (itemized individual contributions) and cm (committee master) for the 1980, 1992, 1996 and 2012 two-year cycles. Washington, DC. URL: https://www.fec.gov/data/browse-data/?tab=bulk-data (visited on 07/25/2026).

Fryer Jr., Roland G. and Steven D. Levitt (Nov. 2012). "Hatred and Profits: Under the Hood of the Ku Klux Klan". *The Quarterly Journal of Economics* 127.4, pp. 1883–1925. DOI: 10.1093/qje/qjs028.

Grammich, Clifford et al. (Nov. 2018). *Longitudinal Religious Congregations and Membership File, 1980–2010 (County Level)*. Dataset. Merges the 1980 and 1990 Churches and Church Membership studies with the 2000 and 2010 Religious Congregations and Membership Studies. Some county units are aggregated; see Bacon, Finke, and Jones (2018) for the merge rules and their limits. DOI: 10.17605/OSF.IO/B6N84. URL: https://doi.org/10.17605/OSF.IO/B6N84.

Green, Lloyd (Mar. 19, 2023). *Birchers Review: How the Republican Far Right Gave Us Trump and DeSantis. Matthew Dallek's Fast-Paced and Well-Researched History Shows How the John Birch Society Rose, Raved and Never Went Away*. Book review. The Guardian. URL: https://www.theguardian.com/books/2023/mar/19/birchers-review-republican-far-right-trump-desantis-dallek-john-birch-society (visited on 08/10/2026).

Jocher, Glenn, Ayush Chaurasia, and Jing Qiu (2023). *Ultralytics YOLOv8*. Version 8.0.0. URL: https://github.com/ultralytics/ultralytics.

Kraft, Charles Jeffrey (1992). "A Preliminary Socio-Economic and State Demographic Profile of the John Birch Society". Undergraduate thesis, Tufts University.

Kuriwaki, Shiro (2026). *Cumulative CES Common Content*. Version V12. Dataset. DOI: 10.7910/DVN/II2DB6. URL: https://doi.org/10.7910/DVN/II2DB6.

Lazar, Ernie (2020). *Schlafly, Phyllis and John Birch Society*. Archival documents including correspondence. URL: archive.org (visited on 03/16/2025).

Li, Minghao et al. (2023). "TrOCR: Transformer-Based Optical Character Recognition with Pre-trained Models". *Proceedings of the AAAI Conference on Artificial Intelligence* 37.11, pp. 13094–13102.

Lin, Tsung-Yi et al. (2014). "Microsoft COCO: Common Objects in Context". In: *European Conference on Computer Vision*. Springer, pp. 740–755.

Madestam, Andreas et al. (Nov. 2013). "Do Political Protests Matter? Evidence from the Tea Party Movement". *The Quarterly Journal of Economics* 128.4, pp. 1633–1685. DOI: 10.1093/qje/qjt021.

Markle, Gerald E., James C. Petersen, and Morton O. Wagenfeld (1978). "Notes from the Cancer Underground: Participation in the Laetrile Movement". *Social Science & Medicine. Part A: Medical Psychology & Medical Sociology* 12, pp. 31–37. DOI: 10.1016/0271-7123(78)90020-2.

McGirr, Lisa (2001). *Suburban Warriors: The Origins of the New American Right*. Princeton, NJ: Princeton University Press.

McVeigh, Rory, David Cunningham, and Justin Farrell (Dec. 2014). "Political Polarization as a Social Movement Outcome: 1960s Klan Activism and Its Enduring Impact on Political Realignment in Southern Counties, 1960 to 2000". *American Sociological Review* 79.6, pp. 1144–1171. DOI: 10.1177/0003122414555885.

Nemeth, Stephen C. and Holley E. Hansen (June 2022). "Political Competition and Right-Wing Terrorism: A County-Level Analysis of the United States". *Political Research Quarterly* 75.2, pp. 338–352. DOI: 10.1177/10659129211006791.
Pape, Robert A., Kyle D. Larson, and Keven G. Ruby (July 2024). "The Political Geography of the January 6 Insurrectionists". *PS: Political Science & Politics* 57.3, pp. 329–339. DOI: 10.1017/S1049096524000040.
Romano, Joseph P. and Michael Wolf (2005). "Stepwise Multiple Testing as Formalized Data Snooping". *Econometrica* 73.4, pp. 1237–1282. DOI: 10.1111/j.1468-0262.2005.00615.x.
Satyanath, Shanker, Nico Voigtländer, and Hans-Joachim Voth (Apr. 2017). "Bowling for Fascism: Social Capital and the Rise of the Nazi Party". *Journal of Political Economy* 125.2, pp. 478–526. DOI: 10.1086/690949.
Schroeder, Jonathan et al. (2026). *IPUMS National Historical Geographic Information System: Version 21.0*. Dataset. Minneapolis, MN. DOI: 10.18128/D050.V21.0. URL: http://doi.org/10.18128/D050.V21.0.
Spruill, Marjorie J. (2017). *Divided We Stand: The Battle over Women's Rights and Family Values That Polarized American Politics*. New York: Bloomsbury.
Tausanovitch, Chris and Lynn Vavreck (2021). *Democracy Fund + UCLA Nationscape, October 10, 2019 – December 23, 2021*. Version 20211215. Dataset. URL: https://www.voterstudygroup.org.
Tkachenko, Maxim et al. (2020). *Label Studio*. https://github.com/heartexlabs/label-studio.
U.S. Bureau of Economic Analysis (2025). *Regional Economic Accounts, Table CAINC1: Personal Income, Population, Per Capita Personal Income, County, 1969–2024*. Dataset. County personal income estimates for reference year $T$ are released in November of $T + 1$; the 1969–2024 vintage used here is the November 2025 release. Suitland, MD. URL: https://apps.bea.gov/regional/downloadzip.cfm (visited on 07/25/2026).
U.S. Census Bureau (2019). *Geographic Relationship Files: 2010 ZCTA–County and 116th Congress ZCTA–Congressional District*. Datasets. Two files of different vintage are cited together: the ZCTA–county file is the 2010 Census relationship release, and the ZCTA–congressional district file is the 116th Congress release. The year given is the later of the two. Suitland, MD. URL: https://www.census.gov/geographies/reference-files.html (visited on 07/25/2026).
— (2020). *2020 ZIP Code Tabulation Area (ZCTA) to County Relationship File*. Dataset. National file tab20_zcta520_county20_natl.txt; each record identifies a 2020 ZCTA–county intersection and reports the land and water area of the intersecting part. Suitland, MD. URL: https://www2.census.gov/geo/docs/maps-data/data/rel2020/zcta520/tab20_zcta520_county20_natl.txt (visited on 08/09/2026).
U.S. National Library of Medicine (2024a). *DailyMed: SKLICE—Ivermectin Lotion*. Drug label. Labeler: Azurity Pharmaceuticals; 0.5 percent lotion for topical use; updated July 11, 2024; Structured Product Labeling set ID 7579bdfe-a538-4bff-b7c7-df2c4b6f13db. Bethesda, MD. URL: https://dailymed.nlm.nih.gov/dailymed/drugInfo.cfm?setid=7579bdfe-a538-4bff-b7c7-df2c4b6f13db (visited on 08/09/2026).
— (2024b). *DailyMed: SOOLANTRA—Ivermectin Cream*. Drug label. Labeler: Galderma Laboratories, L.P.; 1 percent cream for topical use; updated October 24, 2024; Structured

Product Labeling set ID b1d5b166-ab06-4ab5-b0c6-31126238118a. Bethesda, MD. URL: https://dailymed.nlm.nih.gov/dailymed/drugInfo.cfm?setid=b1d5b166-ab06-4ab5-b0c6-31126238118a (visited on 08/09/2026).

Voigtländer, Nico and Hans-Joachim Voth (Aug. 2012). "Persecution Perpetuated: The Medieval Origins of Anti-Semitic Violence in Nazi Germany". *The Quarterly Journal of Economics* 127.3, pp. 1339–1392. DOI: 10.1093/qje/qjs019.

Wu, Yuxin et al. (2019). *Detectron2*. https://github.com/facebookresearch/detectron2.